energy&fuels

pubs.acs.org/EF

Article

Surrogate Reaction Mechanism for Waste Incineration and Pollutant Formation

Corinna Netzer,* Tian Li, and Terese Løvås

Cite This: *Energy Fuels* 2021, 35, 7030–7049

Read Online

ACCESS | Metrics & More | Article Recommendations | Supporting Information

ABSTRACT: The incineration of municipal solid waste (MSW) is an attractive technology to generate thermal energy and reduce landfill waste volume. To optimize primary measures to ensure low emission formation during combustion, numerical models that account for varying waste streams and their impact on nitrogen oxide (NO_x) formation are needed. In this work, the representation of the fuel by surrogate species is adopted from liquid fuel and biomass combustion and applied to solid waste devolatilization and combustion. A surrogate formulation including biomass components, protein, inorganics, and plastic species is proposed, and a comprehensive description of the heterogeneous and homogeneous reactions is developed. The presented work combines and extends available schemes from the literature for woody and algae biomass, coal, and plastic pyrolysis. The focus is set on the prediction of fuel NO_x and its precursors, including cyclic nitrogen-containing hydrocarbons. Additionally, the interaction of NO_x with sulfur and chloride species is accounted for, which are typically released during the devolatilization of MSW. The model allows for predicting thermogravimetric analysis measurement of waste fractions and different waste mixtures. The proposed kinetic mechanism well reproduces NO_x formation from ammonia and hydrogen cyanide and its reduction under selective non-catalytic reduction conditions. The chemical model is successfully applied to predict the released gas composition along a grate-fired fuel bed using a stochastic reactor network.

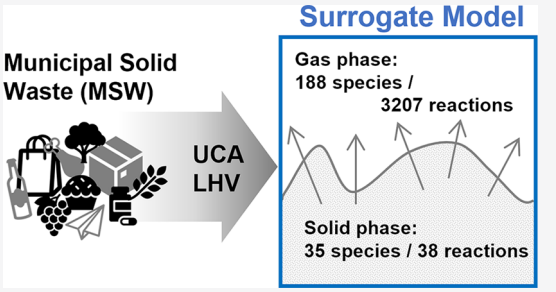

1. INTRODUCTION

Municipal solid waste (MSW) emergence is increasing worldwide and is predicted to grow further in the future.[1] Therefore, efficient waste stream management has become more important from an economic and environmental point of view. Thanks to its benefits over landfills, the capacities of MSW treatment by incineration are growing in China[2] and Europe. For the European market, this development is addressed and supported by the European Landfill Directive.[3] In waste-to-energy (WtE) plants, heat and power is generated from wastes, while at the same time, the mass and volume of the waste that must be landfilled are reduced. Further, the incineration process reduces environmental risks compared to landfills, e.g., by reducing the emission of greenhouse gas methane (CH_4).[4] However, just as with every combustion process, waste incineration emits harmful substances. Nitrogen oxides (NO_x) are of significant concern because they act as an acid rain precursor and in the formation of photochemical smog.[5] MSW contains a wide variety of materials, e.g., food and other organic wastes, different papers, plastics, metals, and composite materials. During combustion of this diverse mixture, corrosive or poisonous species, such as sulfur oxides (SO_x), hydrochloric acid (HCl), and dioxins, are emitted besides typical combustion byproducts and emissions. These emissions are strictly regulated, and flue gases are cleaned according to regulations before released into the atmosphere. To fulfill the rules, primary measures reduce the formed emissions during combustion by control of the operating conditions, such as air staging or reburning, and secondary measures, i.e., cleaning of the flue gases after the combustion, are commonly applied nowadays. Thanks to their high effectiveness, secondary measures are advantageous, but their operation is expensive. Therefore, the additional use of primary measures is still important. To improve primary measures or develop a new low emission methodology, the complex emission formation and their determining factors have to be further investigated. Emission and precursor measurements are carried out to gain further insights. Still, as a result of the large size of waste incineration plants and limited access to the furnaces, species concentration measurements are usually limited to a certain range of the fuel bed and some single selected points in the flue gas. For example, Jepsen et al.[6] and Bøjer et al.[7] reported species measurements above the grate of full-scale WtE plants using water-cooled probes with a length of up to 6 m. Jepsen et al.[6] measured major combustion products and fuel NO_x precursors at four

Special Issue: In Memory of Mario Costa

Received: October 17, 2020
Revised: February 1, 2021
Published: February 11, 2021

points along the grate, and Bøjer et al.[7] detailed corrosive species at five incidences. Razmjoo et al.[8] presented species concentrations within the fuel bed of a comparable small plant and woody residues.

Numerical modeling can help extend the available data by a comprehensive analysis of the combustion process of the combustion chamber. Detailed studies with a focus on NO_x are, e.g., presented by Jell et al.[9] and Frank et al.[10] To investigate the NO_x emission formation, it is clear that the emission chemistry has to be mathematically described and implemented into numerical simulations, starting from devolatilization in the fuel bed to NO_x precursor formation, throughout the entire process to the conditions in aftertreatment units.

The devolatilization kinetics of MSW are usually determined by thermogravimetric (TG) analysis, which measures the weight loss under pyrolysis conditions, and differential thermogravimetric (DTG) analysis, from which reaction rate parameters can be found. The rate of mass conversion can be determined by[11]

$$\frac{d\alpha}{dt} = A \exp\left(\frac{-E_a}{RT}\right)(1-\alpha)^n \quad (1)$$

where A is the frequency factor, E_a is the activation energy, T is the temperature, R is the universal gas constant, α is the mass conversion rate, and t is the time. For the kinetic rate estimation, different approaches are proposed.[11] Examples are the nonlinear least squares algorithm,[12] the Avrami−Eroffev equation,[13] and the modified integral Coats−Redfern method for non-isothermal reaction conditions.[14] Typically, the reaction parameters are determined for a specific waste sample or material, such as juice cartons, wood type, or paper quality. Their decomposition is then described by a global heterogeneous decomposition step and global cracking or decomposition pathways, including tar, gases, and char.[11] This approach is widely used for MSW[12−20] but lacks the flexibility to describe and interchange the solid fuel composition to predict changes in released gas and tar species compositions and emission precursors as a function of varying waste streams. The use of surrogate species and a corresponding detailed chemistry scheme can overcome this descriptive character and direct simulations toward predictive results. The concept of surrogate species is well-established in liquid fuel combustion. In extreme cases, only one surrogate species, e.g., *n*-heptane, represents the hundreds to thousands of different diesel fuel species. The underlying idea is that the surrogate fuel aims to represent the main chemical and physical properties of the true fuel to emulate its combustion behavior. In liquid fuel combustion, this concept is not only used to replicate the commercial fuel in numerical simulations but also to design standard and reference test fuels. In comparison to liquid fuel combustion, solid fuels and, specifically, waste streams are characterized by the variation and heterogeneity of the materials, and consequently, an even larger number of elements and species have to be considered in a modeling approach. The concept of a surrogate fuel has been successfully applied to represent woody biomass by Ranzi and co-workers[21−23] and Anca-Couce and co-workers[24,25] and algae biomass by Debiagi et al.[26] The potential and need for the use of surrogate species in solid fuel combustion are not limited to the solid-phase description but is also needed for the released gas and tar species, as highlighted by Žnidarčič et al.[27] for the simulation of sewage sludge and Mehrabian et al.[28] for biomass simulation. Often, the released gas mixture is represented by syngas or mixtures with up to C_2 species, which are much smaller than expected tar species in solid fuel combustion and, consequently, have different activation energies and ignition delay times and might not include intermediate species that are potential emission precursors. To model MSW, the surrogate blend should represent the main combustion characteristics of the fuel. Desirable properties are (1) the composition according to the ultimate component analysis (UCA), (2) the lower heating value (LHV), and (3) a range of representative tar species, including aromatic and nitrogen-containing species. The UCA composition represents the contents of carbon, hydrogen, and oxygen, which make up most of any waste mixture. Their ratio can be correlated to the lower heating value of the fuel and, therefore, the heat release. According to the UCA, one can also assign nitrogen and corrosive species to the surrogate. The nitrogen content is considered a key characteristic because the dominating NO_x formation pathway is fuel NO_x.[5] The mass contribution of the corrosive species, such as sulfur and chlorine species, is negligible in waste streams. Still, their formation and corrosive characteristics may lead to an upper temperature limit in the waste incineration plants, e.g., in the superheaters, for protective measures. Therefore, the release of corrosive species is linked to the electrical efficiency of plants. Further, sulfur and chlorine have been shown to limit or catalyze the further oxidation of CO[29,30] and interact with NO_x chemistry by their impact on the formation of H, O, and OH radicals.[31−33] They are also involved in joint reaction pathways, nitrosyl chloride formation,[34,35] and reactions between SO_x and NO_x species.[36] These findings suggest that the mathematical description of the gas phase in WtE plants should include those species.

The description of the fuel through a surrogate blend also enables the use of a more detailed description of the gas phase, including tar species. As introduced by Ranzi and co-workers[21−23] for biomass, in such a combination, the gas-phase species and reactions are described by species up to C_{11} and hundreds of reactions. This degree of detail of intermediate species allows for the introduction of models that describe species formation based on available intermediate species, precursors, and the local radical pool. In WtE applications, most NO_x is emitted as nitrogen monoxide (NO), which is formed during combustion, and later under atmospheric conditions oxidized to mainly NO_2, with small amounts of N_2O.[9] NO can be produced by different mechanisms and species. Fuel NO_x is a product of NO_x precursors, such as ammonia (NH_3) and hydrogen cyanide (HCN). The precursors are released during devolatilization and further oxidized to N_2 or NO depending upon the local temperature and stoichiometry. Additionally, some NO can be released directly by the solids in a first initiating step.[5,6] Thermal NO_x contributes less because the local temperatures over the fuel bed of waste incineration plants are usually too low for the thermal NO_x window of 1400−1800 K;[5] hence, thermal NO_x is mainly formed in local hot spots caused by the secondary air injection further up the combustion chamber.[9] To a small amount, NO_x is formed by the N_2O mechanism[37] or via NCN, which is a result of the CH radical break up of the triple bond of N_2 molecules (prompt NO_x).[38] Several detailed gas-phase mechanisms that offer a description of the different NO_x formation mechanisms are available in the

https://dx.doi.org/10.1021/acs.energyfuels.0c03485
Energy Fuels 2021, 35, 7030−7049

literature.[39−44] Respecting the conditions above the fuel bed, they capture the NO_x formation during reburning, staged combustion, and in selective non-catalytic reduction (SNCR) units. However, those schemes do not include corrosive species that can impact the NO_x formation in the free broad of a WtE plant.

In this work, to the best knowledge of the authors, a surrogate formulation for MSW is presented for the first time. The model consists of a comprehensive description of the devolatilization and heterogeneous and homogeneous reactions for solid waste incineration. The model is based on available reports for biomass components from the literature and extended by knowledge to plastic and coal pyrolysis. Furthermore, a method for the surrogate formulation is proposed. The gas-phase chemistry model aims to include representative tar species and NO_x formation, including models for fuel NO_x and interaction reactions with sulfur and chlorine species. The manuscript is structured as follows: first, the selected surrogate species are presented and validated individually. The introduction and validation of species and submodels are split into sections for biomass species, products from reactions with inorganic components, and plastic species. Second, the methodology to formulate surrogate mixtures is presented and validated against composite materials and MSW mixtures. Third, the gas-phase chemistry compilation, including submodels and a model reduction strategy, is discussed. In the last step, the developed reaction scheme is employed to predict the species release along a grate-fired fuel bed of a typical waste incineration plant. For this simulation, a reactor network approach consisting of stochastic reactors that account for solid, pore, and gas-phase kinetics and inhomogeneity within the fuel bed is applied. The prediction is validated against data from the literature for NO_x and its precursors, sulfur, and chlorine species. Before the paper is concluded, the limitations and potentials of the presented approach are discussed.

2. CHEMICAL MODEL

MSW is a heterogeneous mixture of food and other organic waste, different types of paper and cardboard, various plastic components, inorganic species, metals, and composites of those materials. The aim of the developed chemical model for MSW incineration is to describe the gas release of this heterogeneous fuel mixture, the reactions of released gases, and emission formation in the gas phase. The emphasis is on NO_x chemistry, including thermal, fuel, and prompt NO_x pathways and their interaction with sulfur and chlorine species. The solid-phase scheme combines reaction schemes for woody biomass and algae pyrolysis, including reaction products from inorganic species and metaplastics[22] (gaseous species captured in the solid structure), coal conversion, and single plastic species. Metals and glass are neglected because they contribute little to the heat release. Chlorine species with up to 9000 mg/L[45] and sulfur species with up to 130 mg/L[45] are only present in small amounts in MSW, but their species are linked to NO chemistry[31−36] and, therefore, need consideration. Hence, the included elements are carbon (C), oxygen (O), hydrogen (H), nitrogen (N), chlorine (Cl), sulfur (S), and silicon (Si) (ash).

The developed chemical model is based on the scheme by Ranzi et al.,[22] which provides the modeling of devolatilization of woody biomass and the subsequent reactions in the gas phase. The heterogeneous reaction scheme is extended with nitrogen-containing species to model fuel NO_x formation from biomass and plastic components, by a plastic containing chlorine, and species that account for the release of sulfur- and nitrogen-containing products of heterogeneous reactions with inorganics. The gas-phase mechanism is correspondingly extended to contain NO_x and NO_x precursor chemistry (NH_3 and HCN) and cyclic nitrogen-containing species, sulfur, and chlorine chemistry. The model components are chosen according to the following criteria: (1) well-validated in the literature, (2) a small absolute number of species and reactions, and (3) if possible, from the same research group for consistency. The extension for the solid-phase description is presented, followed by the proposed surrogate formulation and the gas-phase scheme.

2.1. Heterogeneous Reactions. A MSW mixture can be divided into material fractions. The fractions considered in the presented model are food and organic wastes, textiles, papers and cardboard, plastics, and inorganic components. Food and organic leftovers are modeled using surrogate species for woody biomass and protein.

Food waste, such as vegetables and fruits, meat, and other organic waste (e.g., resulting from landscaping and gardening, wood chips, and wooden consumer goods) include to a large extent the basic modules of plants, which are cellulose, hemicellulose, and lignin. Green biomass, fruits, seeds, and meat also contain protein, starches, sugars, and lipids. From this group, only proteins are included in the model. Starches, sugars, and lipids have the same concentrations in a MSW mixture as the wood components mentioned above. Still, they do not release significantly different tar and gas species but mainly oxygen-containing tar species, small aromatic species, and typical pyrolysis products (H_2, CH_4, and C_2H_4)[26] nor do they contribute to critical phenomena, such as the fuel NO_x formation from nitrogen-containing species, such as, e.g., protein. Textiles and papers are bio-derived materials that contain to a large extent wooden fibers. Hence, woody biomass surrogate species can also represent these materials. Plastics release a significant amount of aromatic species and have different functional groups than bio-derived streams. They typically do not include oxygen or, if so, only in little amounts but can consist of nitrogen or chlorine functional groups depending upon their application purpose. The model consists of the most common plastics in MSW streams [polyethylene (PE), polypropylene (PP), and polystyrene (PS)] but also polyamide (PA) and polyvinyl chloride (PVC) to model fuel NO_x and chlorine release, respectively. Inorganic waste components are not directly modeled in the presented scheme, but their product gases of heterogeneous reactions are included. In this way, e.g., the sulfur content of a MSW mixture can be modeled. Modern products and wastes are often composites. For example, newspapers, including mainly wood fibers and inorganic components in the printing ink, and packaging or wrappings, have several layers made of paper, plastics, metals, and glue. The surrogate concept assumes that those materials can be represented by a mixture of the previously mentioned surrogate species that capture the overall combustion behavior, release representative tar species, and mimic the emission characteristic of those materials.

The presented mathematical description of the waste surrogate is based on simplified single- and multi-step reactions to describe devolatilization. Still, the model is based on the concept of experimentally derived apparent reaction rates, but instead of determining these apparent

https://dx.doi.org/10.1021/acs.energyfuels.0c03485
Energy Fuels 2021, 35, 7030−7049

reaction rates for a specific MSW mixture, the rates describe the decomposition of single surrogate species. This concept allows for the combination of the surrogate species to represent any waste mixture flexibly. Consequently, the solid-phase scheme consists of a much lower number of species and reactions than that of the detailed gas-phase model, which follows kinetic measurements and fundamental rate estimations for elementary reactions. The main aim of the developed surrogate and solid-phase model is to model the mass conversion from solid to gas phase accurately and to provide representative key characteristics of the released gases, which are different tar types, nitrogen- and oxygen-containing and aromatic species, other functional groups following the concept of group contribution methods, and emission precursors (NH_3, HCN, sulfur, and chlorine species). All surrogate species and their primary purpose in the surrogate model are listed in Table 1.

2.1.1. Biomass Surrogate Species. For the biomass fraction, the reaction scheme by Ranzi et al.,[22] which includes 18 species and 23 reactions, builds the base and is adopted here entirely and unchanged. The included surrogate components are cellulose (CELL), hemicellulose (HCE), and lignin species with different C/H/O ratios denoted LIG_C, LIG_H, and LIG_O. Further, gaseous species trapped in the solid phase (metaplastics), G{CO}, G{CO_2}, G{COH_2} and G{H_2}, char (C_S), and moisture (H_2O_S), are comprehended. The nitrogen content in biomass wastes is represented by the suggested surrogate species for algae pyrolysis by Debiagi et al.[26] From this scheme, the protein PROT ($C_{400}H_{900}O_{150}N_{86}$) is chosen because it releases a larger amount of NH_3 than HCN, which corresponds to the ratio found in MSW mixtures. For this implementation, the set of metaplastics is extended by G{NH_3} and G{HCN}.[26] The reactions are given in Table 2. Please note that the reactions by Debiagi et al.[26] include the species TAR_N ($C_{13}H_{15}O_3N_4$) that is assumed to be an equimolar combination of C_4H_5N, C_5H_4ON, and $C_4H_6O_2N_2$. For the oxygen-containing species, no suitable gas-phase chemistry is available in the literature. However, for the representation of nitrogen-containing tar species released during coal pyrolysis, pyridine and pyrrole are suggested,.[47] From liquid fuel combustion, detailed reaction schemes for both species are available in the literature, for pyridine (C_5H_5N) by Alzueta et al.[48] and for pyrrole (C_4H_5N) by Wu et al.[49] Toward the use of those gas-phase mechanisms, TAR_N is replaced here by

$$TAR_N = HCN + NO + pyrrole + pyridine + C_3H_4O_2 \quad (2)$$

To balance the stoichiometry, HCN and NO are chosen because they are present in the decomposition reactions for proteins[26] and $C_3H_4O_2$. $C_3H_4O_2$ is employed because it is present in the gas-phase mechanism by Ranzi et al.,[22] so that no other gas-phase reactions have to be added to represent the ketone group, following the concept of group contribution theories. This reformulation of the decomposition reaction of TAR_N results in a 35% decrease in the heat of combustion of the product mixture. However, because only 0.09 mol of TAR_N is formed per mole of PROT, this reduction is considered acceptable here.

The mass loss under thermogravimetry (TG) conditions is validated against experiments available in the literature for all biomass surrogate species. For this comparison, the stochastic gasification module available within LOGEreserach version 1.0[52] and introduced by Weber et al.[53] is employed. In this model, the reactor volume is discretized into non-dimensional virtual packages, called stochastic particles. Each of the stochastic particles contains a certain amount of solid mass, pore gas in the solid, and bulk gas. During a stochastic mixing step, the bulk gas of randomly selected particles is mixed to their mean. Heat can be transferred from the reactor walls, which serve as boundary conditions, and between solid particles. The heat transfer coefficients are calculated using Nusselt laws. In each time step, the chemistry is integrated

Table 1. Solid Surrogate Species

species	description	reference reactions	reference reaction rates
	Biomass Species		
cellulose, CELL	biomass component	Ranzi et al.[22]	Ranzi et al.[22]
hemicellulose, HCE	biomass component	Ranzi et al.[22]	Ranzi et al.[22]
lignin, LIG_O	lignin rich in oxygen	Ranzi et al.[22]	Ranzi et al.[22]
lignin, LIG_H	lignin rich in hydrogen	Ranzi et al.[22]	Ranzi et al.[22]
lignin, LIG_C	lignin rich in carbon	Ranzi et al.[22]	Ranzi et al.[22]
protein, PROT	nitrogen content in biomass	Debiagi et al.[26]	Debiagi et al.[26]
	Inorganic Species[a]		
CO_2i	release of CO_2 from inorganics	Debiagi et al.[26]	Debiagi et al.[26]
NH_3i	release of NH_3 from inorganics	Debiagi et al.[26]	Debiagi et al.[26]
(H_2S SO_2 COS)i	release of H_2S, SO_2, and COS		
	Plastic Species		
polyethylene, PE	typical plastic species		Wu et al.[46]
polypropylene, PP	typical plastic species		Wu et al.[46]
polystyrene, PS	high release of aromatics		Wu et al.[46]
polyamide, PA	fuel NO from plastics		Herrera et al.[47]
polyvinyl chloride, PVC	release of HCl		Wu et al.[46]
	Other Species		
H_2O(S)	moisture content	Ranzi et al.[22]	Ranzi et al.[22]
ash	ash content fuel	Ranzi et al.[22]	Ranzi et al.[22]

[a]The term "inorganic species" here means representative surrogate species that account for the release of product gases of heterogeneous reactions of inorganic species with the gas phase. The inorganic species themselves and their reactions are not included in the model description.

Table 2. Protein Species and Reactions Included in the Solid-Phase Mechanism[a]

reaction	A (s^{-1})	n	E_a (kJ/mol)
PROT → 5$PROT_2$ + 27NH_3 + 7HCN + 20.75G{H_2} + 21.5CH_4 + 70C_2H_4 + 23.5H_2O + 0.5NO + 0.5pyrrole + 0.5pyridine + 0.5$C_3H_4O_2$	1.00×10^4	0.00	64.9
$PROT_2$ → 27char + 2$char_N$ + 1.0833C_6H_6 + 3G{NH_3} + 1.5G{CO} + 22H_2O + 0.5pyrrole + 0.5pyridine + 0.5$C_3H_4O_2$ + 0.5NO	1.00×10^3	0.00	62.8

[a]Reactions and rates by Debiagi et al.[26]

https://dx.doi.org/10.1021/acs.energyfuels.0c03485
Energy Fuels 2021, 35, 7030−7049

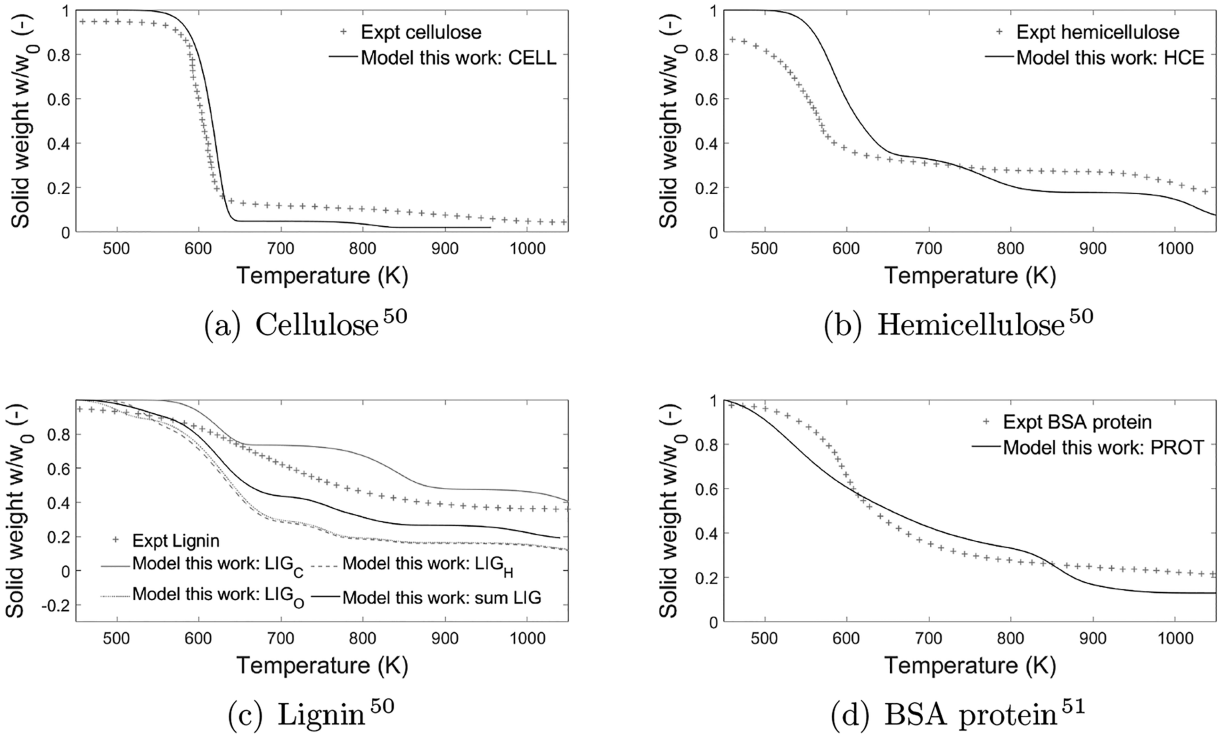

Figure 1. TG experimental curves at 5 K/min for cellulose, hemicellulose, and lignin by Zhao et al.[50] and at 10 K/min for BSA (albumin and bovine) protein by Francisca et al.[51] Model predictions show the solid mass loss of the corresponding initialized surrogate species (given in the legends) over the temperature range of 500−1000 K.

within each of the stochastic particles. In this chemistry step, the devolatilization reactions, surface reactions, and gas-phase kinetics are solved. The solid mass is reduced using the reaction source rates of drying, devolatilization, and heterogeneous reactions. According to the calculated mass loss, the representative diameters of the solid particles are updated. For a detailed discussion and the solved set of equations, the reader is referred to Weber et al.[53] and Netzer et al.[54] For the chemistry model validation, a set of simulations for each surrogate species is carried out. For these simulations, the solid mass is set to consist of one surrogate species only. The temperature within the reactor is initialized by 300 K, and the wall temperature is initialized by 2000 K. In the model, the bulk gas and solid mass are heated by radiation from the wall and heat transfer between random selected stochastic particles. The heating results in a fixed rate of 12.5 K/min. For the simulations, reactors with a volume of 1 L are chosen. The initial solid mass is set to 10 mg, and the air flow rate is set to 1.15 g/s. During the simulation, the initialized surrogate species will be transformed as specified in the reaction mechanism; e.g., HCE first transforms to HCE_1 and HCE_2, which then result in tar and gas species, metaplastics, and char. For the tree lignin surrogate species, their equimolar weighted sum, denoted by "sum LIG" in Figure 1c, is compared to the measurement rather than the single surrogate species. Figure 1 shows that, for all biomass surrogate species, the weight loss (actual mass over initial mass, w/w_0) is predicted well compared to the experiments.

2.1.2. Inorganic Surrogate Species. To account for the gas products from heterogeneous reactions of inorganic species, the model for CO_2 and NH_3 release of algae biomass by Debiagi et al.[26] is added to the reaction set. For MSW waste, a more considerable amount of NH_3 is usually released than NO.[6,9] This ratio is reflected in the model by changing the species G{NH_3 NO} in the scheme by Debiagi et al.[26] to account only for NH_3 release. The new species is denoted with NH_3i, and released NH_3 can form NO in the gas phase downstream. The reaction rate is adopted unchanged. In analogy, a compound to model the release of sulfur species is formulated in this work using knowledge from coal pyrolysis and combustion. In coal, sulfur is bonded in inorganic, mostly FeS_2, and organic structures. The amount of inorganic bonded sulfur is 50−70% larger than the organic amount.[55] During pyrolysis and combustion conditions, FeS_2 is reduced through heterogeneous reactions at low temperatures (600−650 K) by O_2, at temperatures of >750 K by H_2, at temperatures of >1050 K by CO, and at temperatures of >1250 K by C atoms.[55]

$$FeS_2 + O_2 \rightarrow FeS + FeSO_4 + Fe_2(SO_4)_3 + Fe_2O_3 + SO_2 \quad (3)$$

$$FeS_2 + H_2 \rightarrow FeS + H_2S \quad (4)$$

$$FeS_2 + CO \rightarrow FeS + COS \quad (5)$$

$$FeS_2 + C \rightarrow Fe + CS_2 \quad (6)$$

As a result of the small amount of sulfur in coal (<3 wt %) and waste mixtures (<1.5 wt %[56]), all sulfur is in the developed reaction scheme modeled by a surrogate species and the iron-containing species are not included. In analogy to the species CO_2i and NH_3i, the species (H_2S SO_2 COS)i is formulated. In a two-step reaction pathway from this species, SO_2, H_2S, and organic COS are released to the gas phase. Duan et al.[57] measured released sulfur species from coal in nitrogen (N_2) and carbon dioxide (CO_2) atmospheres and found for different temperatures (973−1273 K) an increasing

https://dx.doi.org/10.1021/acs.energyfuels.0c03485
Energy Fuels 2021, 35, 7030−7049

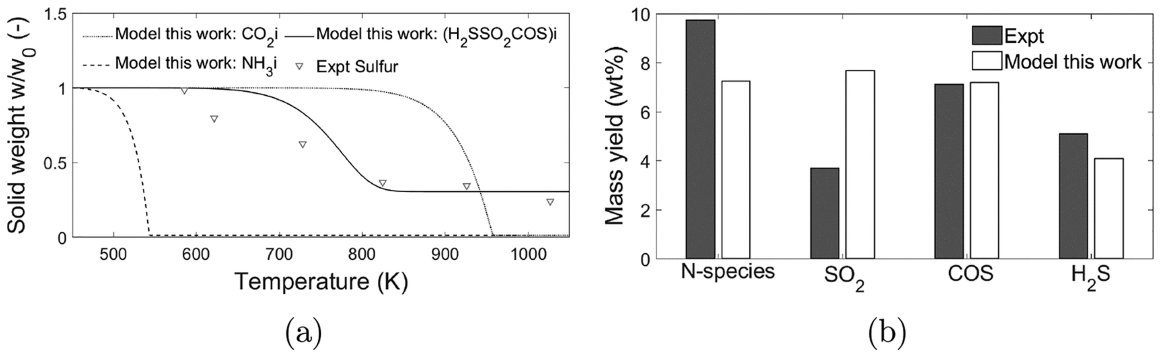

Figure 2. Model predictions of the solid mass loss for the inorganic species and mass yield in coal pyrolysis: (a) measured mass loss of sulfur in fixed-bed pyrolysis of raw Bowman's coal at different temperatures by Zhou et al.[58] and (b) experimental results for pyrolysis yields of sulfur-containing species in a CO_2 atmosphere by Duan et al.[57] at 1073 K.

Table 3. Surrogate Species Representing Gas Products from Inorganic Species Reactions

reaction	A (s^{-1})	n	E_a (kJ/mol)
CO_2i[26] → CO_2	1.00×10^7	0.00	159.0
NH_3i[26] → NH_3	2.50×10^{10}	0.00	116.3
$(H_2S\ SO_2\ COS)i \rightarrow (H_2S\ COS)i + SO_2$	1.00×10^5	0.00	100.0
$(H_2S\ COS)i \rightarrow H_2S + COS$	1.00×10^3	0.00	60.0

trend in released SO_2, H_2S, and COS. It should be noted that, even though oxygen is not present in either pyrolysis atmospheres, SO_2 is found in the product gases. The total amount of those species is within ±2% in mass yield, similar to each other. Therefore, in the present model, the species are assumed to be released in the same amount and CS_2 is omitted. As a result of the findings and assumptions, the release of sulfur species is formulated as

$$(H_2S\ SO_2\ COS)i \rightarrow (H_2S\ COS)i + SO_2 \quad (7)$$

$$(H_2S\ COS)i \rightarrow H_2S + COS \quad (8)$$

The reaction rates are set to replicate the measurement by Zhou et al.,[58] as shown in Figure 2, and they are given in Table 3. For comparison, Figure 2 also shows the predicted mass loss for CO_2i and NH_3i and will be further discussed in the Application section. Figure 2b shows the mass yield of the released sulfur and nitrogen species from coal. Coal is modeled here by the mixture NH_3i = 1.56, CO_2i = 0.04, $(H_2S\ SO_2\ COS)i$ = 4.0, C_S = 74.96, G{CO} = 7.63, G{COH_2} = 7.41, and G{H_2} = 4.39 in mass percentage to fulfill the UCA measurement reported by Duan et al.[57] In the experiment, the mass yield of coal pyrolysis in a CO_2 atmosphere was measured. HCN was measured and reported, while in the model, NH_3 is released.

2.1.3. Plastic Surrogate Species. The plastic fraction is modeled to contain the most common plastic species in MSW, i.e., polyethylene (PE), polypropylene (PP), polystyrene (PS), and polyvinyl chloride (PVC). A polyamide (PA) species, here polycaprolactam also called nylon 6, is chosen to account for nitrogen-containing compounds. The main structural groups of the included plastics are shown in Figure 3. TG measurements show that these plastics can be divided into two groups. The first group includes PE, PP, PS, and PA. These plastics are devolatilized over a relatively short interval of 100 K with no solid residue.[59] In contrast, the second group, which includes halogenated plastics, in this work, PVC only, has a more complex devolatilization behavior over a broader range of temperatures, with a double-step weight loss

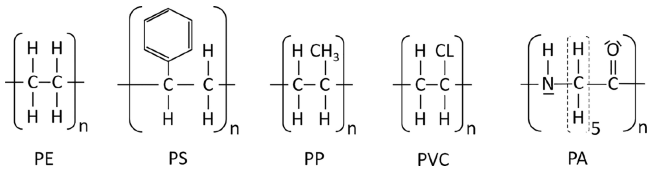

Figure 3. Overview of the structural groups of the considered plastics.

and residue formation.[59] Detailed chemical considerations describing the pyrolysis of plastics, including radical formation, propagation, and determination reactions, and different polymer structures are available for PE,[42] PS,[60] PP,[42] and PVC.[59,61] However, such models are very complicated and not feasible to be incorporated in this work. Hence, for the first group of plastics (PE, PP, PS, and PA), a one-step devolatilization reaction is formulated using the concept of apparent reaction rates that replicates the gas release from experiments on a global level. While reaction rates for these apparent one-step reactions are available in the literature,[15,46,47] models for their stoichiometry are not reported. Therefore, their decomposition reactions are formulated using measurements from literature and, if possible, gas-phase species in the reaction scheme by Ranzi et al.[22] to keep the total number of species and reactions to a minimum. Various tar and gas species are released from plastics as a function of the devolatilization temperature. Generally, the released tar fraction (>C_5) contains between 70 and 99 wt % aromatic species and between 0.5 and 22 wt % non-aromatic species.[62] About 80 wt % C_5−C_9 species are constituting the major part, while larger species are about 20 wt %.[62] In experiments, the identified hydrocarbons are benzene, toluene, naphthalene, their methyl appearance, and cycloalkanes and alkanes up to C_{10}.[63] The gas fraction contains among others about 8 wt % methane (CH_4), 10 wt % ethane (C_2H_6),10 wt % ethene (C_2H_4), 30 wt % C_3 species, 20 wt % C_4 species, 10 wt % C_5 species, and 10 wt % C_6 species.[62] The reactions in the presented model are formulated to represent those ratios of tar and gas species. Their formulation represents a general

https://dx.doi.org/10.1021/acs.energyfuels.0c03485
Energy Fuels 2021, 35, 7030−7049

Table 4. Pyrolysis Products in Weight Percentage[a]

	literature			model formulation		
	tar	gas	solid	tar	gas	solid
PE	51−95	5−24.2	0−7.5	65	33	2
PS	89.5−90	2.5−10	0−4	89	10	1
PP	48−92	4−49.5	0.12−13	49	50	1
PA	30.9−40.8	40.1−63.8	0	60	39	1
PVC	12.3−12.79	58−87, including HCl	30	12	74	13

[a]Data for PE, PS, PP, and PVC are from Anuar Sharuddin et al.,[63] and data for PA are taken from Michal et al.[64] (PA-6 and PA-7 at 1043 K).

composition under the assumption that larger tar species are fast enough broken up to be negligible. Consequently, species such as toluene, styrene, and larger alkanes are neglected to keep the size of the mechanism low, given that their consideration needs a detailed set of gas-phase reactions. However, following the concept of group contribution methods, their structural groups (methyl group and aromatic ring) are represented using species included in the gas-phase scheme. The main included species are small hydrocarbons C_2H_4, CH_4, and I-C_5H_{10} and aromatic species benzene (C_6H_6) and naphthalene ($C_{10}H_8$). Furthermore, the cyclic nitrogen-containing species pyridine (C_5H_5N) and pyrrole (C_4H_5N) are included to model PA. Further, HCl is included to model the decomposition pathway of PVC. Small species [HCN, NO, H_2, and char (C_S)] are used to align the stoichiometry. Their speciation represents the known ratio of released tar (oil), gas, and solid fractions from pyrolysis experiments summarized by Anuar Sharuddin et al.[63] and given in Table 4. For this derivation, all species with a molecular mass larger than C_6H_6 are considered to be tar. Char represents the solid phase, and all remaining species are assigned to gas species. Note that, in the devolatilization reactions, the same product composition is released for all temperatures and equivalence ratios. Still, the tar species are cracked and oxidized following the detailed gas-phase reactions for the local conditions.

PE is known to release aromatic species and small hydrocarbons. Here, they are modeled by benzene (C_6H_6) and naphthalene ($C_{10}H_8$) and by the structural main group C_2H_4 of PE and methane, respectively. The presented model does not distinguish between high-density polyethylene (HDPE) and low-density polyethylene (LDPE). They differ in the number of links between the polymer chains and, therefore, properties, such as density, ductility, or tenacity. However, their main polymer chain $(CH_2{-}CH_2)_n$ and stoichiometry are the same. For the formulation of the speciation reaction, five units ($n = 5$) of the structural element of PE $(CH_2{-}CH_2)_n$ are used.

$$(CH_2{-}CH_2)_5 \rightarrow 0.25C_2H_4 + 2.25CH_4 + 0.75C_6H_6 + 0.25C_{10}H_8 + 1.75H_2 + 0.25C_S \quad (9)$$

Gases released by PS have the highest amount of tar species and the lowest amount of gas (Table 4) as a result of the phenyl constellation in its structural group $(CHC_6H_5{-}CH)_n$ (Figure 3). In the scheme, this is modeled by a higher amount of benzene and naphthalene compared to PE and 2-methyl-2-butene (I-C_5H_{10}) instead of methane.

$$(CHC_6H_5{-}CH_2)_5 \rightarrow 0.5\text{I-}C_5H_{10} + 0.6C_2H_4 + 3C_6H_6 + 1.8C_{10}H_8 + 0.1H_2 + 0.3C_S \quad (10)$$

In addition to the aromatic species, PP produces *n*-propyl ($CHCHCH_3$) and 2-methyl-2-butene to represent species with a methyl group $(CHCH_3{-}CH_2)_n$.

$$(CHCH_3{-}CH_2)_5 \rightarrow 0.5\text{I-}C_5H_{10} + 1.25CH_4 + 0.5C_6H_6 + 0.5C_{10}H_8 + 4H_2 + CHCHCH_3 + 0.25C_S \quad (11)$$

The amide group in PA includes nitrogen and oxygen atoms that are not present in the previously discussed plastics. From experiments, it is known that, under pyrolysis conditions, nylon 6 releases mainly caprolactam ($C_6H_{11}NO$).[47] For the same reasons as discussed for the protein species, this cyclic component is represented by pyridine (C_5H_5N) and pyrrole (C_4H_5N) in the model. This assumption is introduced to keep the gas-phase chemistry scheme reasonably small and aim for the release of fuel NO_x precursors. Because pyridine and pyrrole do not contain oxygen, additional species from the gas-phase mechanism by Ranzi et al.[22] are chosen: ketene (CH_2CO) representing the ketone group as well as CO and NO to balance the stoichiometry. The functional group $(NH{-}[CH_2]_5{-}CO)_n$ is decomposed into

$$(NH{-}[CH_2]_5{-}CO)_5 \rightarrow 2C_4H_5N + C_5H_5N + CO + 4H_2 + 2CH_2CO + 5.53CH_4 + 2NO + C_6H_6 + 0.5C_S \quad (12)$$

The reaction rates measured by Wu et al.[46] for PE, PP, and PS and Herrera et al.[47] for PA are employed. The discussed reactions for plastics and their rates are summarized in Table 5. The same simulations as introduced for the biomass species are performed using stochastic reactors and initializing only one surrogate species. The predicted weight loss captures the measured TG curves well in Figure 4. Note that the plastics are modeled with a single decomposition reaction and that, in the setup of the gasification module, it is solved for the steady-state solution for the set temperature. Hence, the model setup does not account for the dependency upon the heating rate.

PVC has a more complex decomposition behavior than the previously discussed plastics. In the first step, during the dehydrochlorination, HCl and solid polyene structures are released.[61] During this process, benzene, naphthalene, and phenanthrene $C_{14}H_{10}$ are released in addition to HCl.[61] In the second step, the polyene molecules rearrange in the melt, form char residues, and release tar species. In this step,

https://dx.doi.org/10.1021/acs.energyfuels.0c03485
Energy Fuels 2021, 35, 7030−7049

Table 5. Decomposition Reaction Plastic Species[a]

reaction	A (s^{-1})	n	E_a (kJ/mol)
PE → $0.25C_2H_4$ + $2.25CH_4$ + $0.75C_6H_6$ + $0.25C_{10}H_8$ + $1.75H_2$ + $0.25C_S$	1.20×10^{12}	0.63	206.3
PS → $0.5I\text{-}C_5H_{10}$ + $0.6C_2H_4$ + $3C_6H_6$ + $1.8C_{10}H_8$ + $0.1H_2$ + $0.3C_S$	5.00×10^{10}	0.50	172.0
PP → $0.5I\text{-}C_5H_{10}$ + $1.25CH_4$ + $0.5C_6H_6$ + $0.5C_{10}H_8$ + $4H_2$ + $CHCHCH_3$ + $0.25C_S$	6.30×10^{10}	0.90	216.8
PA → 2pyrrole + pyridine + CO + $4H_2$ + $2CH_2CO$ + $5.53CH_4$ + 2NO + C_6H_6 + $0.5C_S$	1.50×10^{11}	0.82	210.8
PVC → $0.9PVC_1$ + $0.1PVC_2$	1.00×10^{10}	0.00	129.7
PVC_1 → PVC_3 + 5HCl	1.50×10^{12}	1.50	163.6
PVC_2 → $0.4PVC_3$ + C_6H_6 + 5HCl	1.50×10^{15}	0.00	190.0
PVC_3 → $2C_2H_4$ + $0.25C_{10}H_8$ + $3.5C_S$	4.80×10^{16}	0.00	266.9

[a]Reaction rates according to Wu et al.[46] and Herrera et al.[47]

alkanes, species with one aromatic ring (e.g., toluene, xylene, and styrene), and polyaromatic hydrocarbons (PAHs) are found in measurements.[59,61,66] A one-step reaction cannot describe this behavior as for the other plastics. Anthony[66] proposed a five-step mechanism

$$A \rightarrow B + HCl \quad (13)$$

$$B \rightarrow C \quad (14)$$

$$B \rightarrow \text{volatiles} \quad (15)$$

$$C \rightarrow D + \text{volatiles} \quad (16)$$

$$D \rightarrow \text{volatiles} \quad (17)$$

and Wu et al.[46] proposed a four-step mechanism

$$A \rightarrow C + \text{gas} \quad (18)$$

$$B \rightarrow C + \text{gas} \quad (19)$$

$$C \rightarrow \text{gas} \quad (20)$$

$$C \rightarrow \text{char} \quad (21)$$

Hereby, A, B, C, and D are different solid species. The two proposed reaction schemes are combined in this work. In the first step, PVC is split into PVC_1 and PVC_2, representing A and B in the scheme of Wu et al.[46] and in an analogy of the hemicellulose decomposition of Ranzi et al.[21,22]

$$PVC \rightarrow 0.9PVC_1 + 0.1PVC_2 \quad (22)$$

Equations 13, 14, 15, 18, and 19 are combined to account for the dehydrochlorination. PVC_1 and PVC_2 both undergo dehydrochlorination, forming a solid residue, which is dehalogenated and named here PVC_3. During this step, PVC_1 frees HCl and PVC_2, additionally C_6H_6.

$$PVC_1 \rightarrow PVC_3 + 5HCl \quad (23)$$

$$PVC_2 \rightarrow 0.4PVC_3 + C_6H_6 + 5HCl \quad (24)$$

The solid residue PVC_3 decomposes in the next step into an alkene (C_2H_4), the two aromatic-ring containing naphthalene, and char (C_S). For this step, equations 16, 20, and 21 are combined.

$$PVC_3 \rightarrow 2C_2H_4 + 0.23C_{10}H_8 + 3.5C_S \quad (25)$$

The further oxidation of char is accounted for in the biomass scheme by Ranzi et al.[22] The reaction rates by Wu et al.[46] are adopted for the PVC decomposition steps. Figure 5 shows the predicted weight reduction and the mass release rate of the

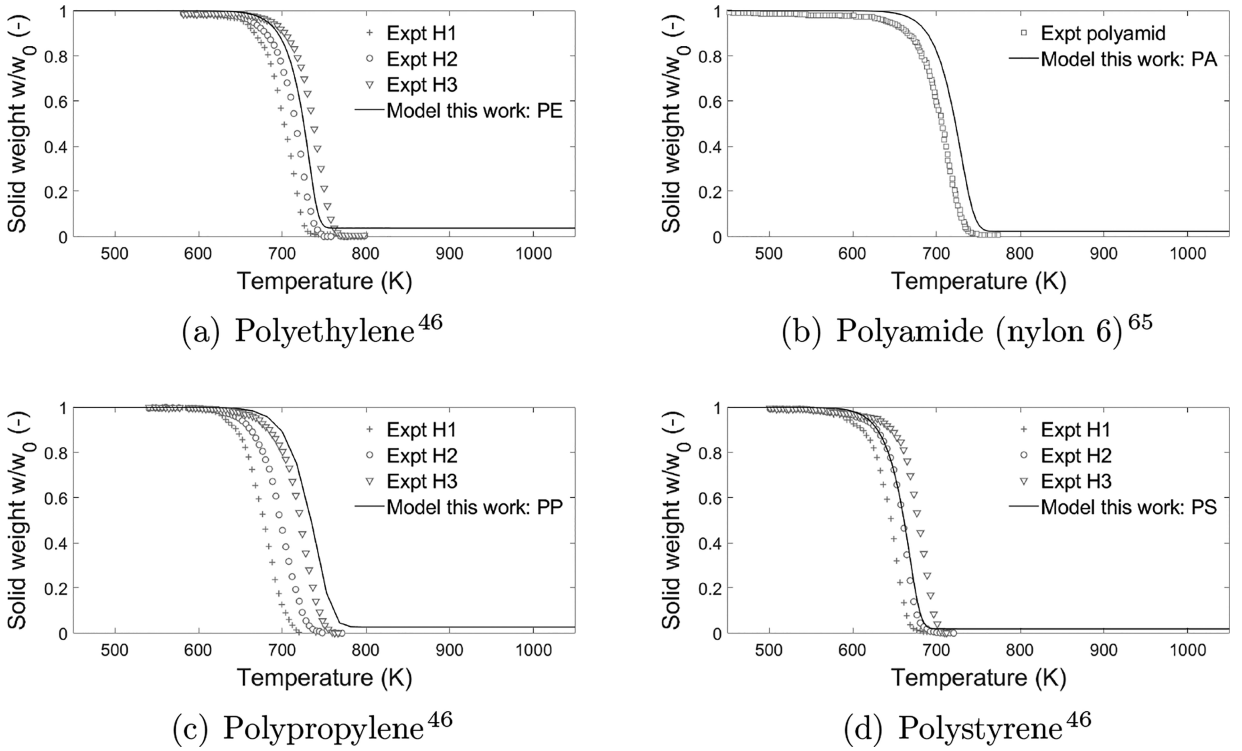

Figure 4. TG experimental curves at 1 K/min (H1), 2 K/min (H2), and 5.5 K/min (H3) for low-density polyethylene, polypropylene, and polystyrene by Wu et al.[46] and at 10 K/min for nylon 6 by Bockhorn et al.[65] Model predictions show the solid mass loss of the corresponding initialized surrogate species (given in the legends) over the temperature range of 500−1000 K.

https://dx.doi.org/10.1021/acs.energyfuels.0c03485
Energy Fuels 2021, 35, 7030−7049

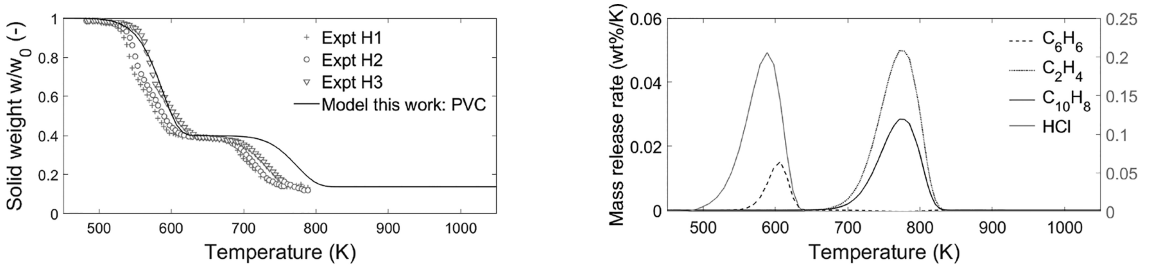

(a) Polyvinylchloride[46] (b) Predicted gas release rates, values for HCl on right y-axis

Figure 5. TG experimental curves at 1 K/min (H1), 2 K/min (H2), and 5.5 K/min (H3) for polyvinylchloride by Wu et al.[46] and model prediction of the (a) solid mass loss and (b) release rate of the gaseous model components.

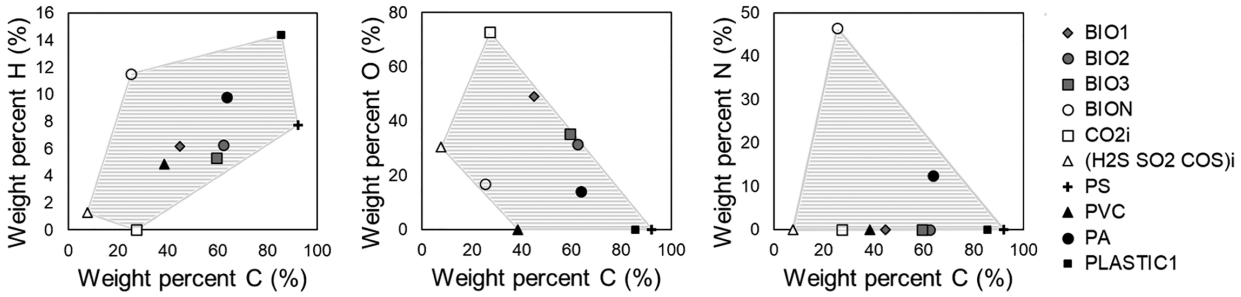

Figure 6. Visualization of the grid point for the linear least square fit used for the surrogate formulation and their covered areas in the hydrogen/carbon, oxygen/carbon, and nitrogen/carbon spaces.

Table 6. Components of Biomass and Waste Fuels and Their Surrogates[a]

	C	H	O	N	Cl	S	ash	moisture	LHV
birch[68]	50.2	7.5	39.9	0.5		0.5	0.3	6.5[15]	18.5
surrogate	51	6.1	40.6	1.2		1.1	0.3	6.5	17.6
spruce[12]	47.4	6.3	46.2	0.7			0.2	6.9[15]	17.9
surrogate	43.9	5.7	42.7	0.5			0.2	6.9	16.6
oil shale (OS)[17]	12.1	2.4	14.4	0.6		1.6	68.8		
surrogate	12.5	1.7	14.5	0.7		1.7	68.8		14.9
newspaper (NP)	51.1	5.9	41.9	0.1			8.1	1.0	17.8
surrogate	51.8	6.1	41.6	0.3		0.2	8.1	1.0	19.3
cardboard (CB)[12]	48.6	6.2	45	0.1		0.1	8.4		16.9
surrogate	44.5	5.6	41.2	0.1		0.1	8.4		16.6
paper sludge (PS)[18]	16.5	1.6	20.2	0.7		1.4	59.6		
surrogate	16.5	1.6	20.2	0.7		1.4	59.6		12.7
MSW1[17]	42.0	5.7	36.6	1.2	7.9	0.2	7.6		
surrogate	41.3	5.6	31.6	1.0	13.7	0.2	6.6		18.5
MSW2[18]	44.7	6.0	33.72	1.7	7.5	0.7	6.7		
surrogate	47.5	5.8	29.4	1.5	12.8	0.6	5.8		19.5
MSW3[6]	31.2	4.4	18.4	1.1	0.7	0.2	16.6	27.5	13.5
surrogate	31.1	4.4	18.4	1.1	0.7	0.2	16.6	27.5	13.4

[a]Values in wt % and LHV in MJ/kg. Values for MSW1 and MSW2 are recalculated to account for chlorine.

gas-phase species. Both predictions align well with the TG measurements and with the reported release ranges by Anthony:[66] HCl is released over 520−660 K; benzene is released over 550−650 K; and toluene and alkanes are released over 660−830 K.

2.2. Surrogate Formulation. A linear least squares fit is applied to optimize the surrogate composition toward UCA measurements to compose the surrogates. The optimization toward the UCA composition is beneficial, first, because the lower heating value (LHV) is correlated to the elementary composition, which is important for the heat released during combustion, and second, because the amount of sulfur and chlorine directly give the amount of necessary (H_2S SO_2 COS)i and PVC, respectively, while the other species can be used to fit the amount of carbon, hydrogen, and nitrogen. For the least squares fit, the species mass fractions Y_i are required to fulfill $0 \leq Y_i \leq 1$ and $\sum Y_i = 1$. For the fit, some of the surrogates are merged to control their ratio. The biomass species are combined (Bio_1, Bio_2, and Bio_3) using the corner points in the C−H space mixing triangle proposed by Cuoci et al.[67] An equal contribution of the nitrogen content from protein and inorganics in biomass is assumed (Bio_N). Further,

https://dx.doi.org/10.1021/acs.energyfuels.0c03485
Energy Fuels 2021, 35, 7030−7049

Table 7. Surrogate Specification Corresponding to Table 6[a]

	birch	spruce	OS	NP	CB	PS	MSW1	MSW2	MSW3
CELL	0.3043	0.3196	0.1501	0.3041	0.4254	0.0992	0.2898	0.2231	0.124
HCE	0.2029	0.2131	0.1001	0.2027	0.2836	0.0661	0.1932	0.1488	0.0827
LIGC	0.0754	0.0591		0.0782	0.0404	0.0176	0.0011	0.0070	
LIGH	0.3017	0.2363		0.2209	0.1617	0.0001	0.0025	0.0164	
LIGO				0.0919		0.0704	0.0018	0.0116	
PROT	0.0157	0.0035	0.0097	0.0039	0.0015	0.0097	0.0060	0.0128	
NH_3i	0.0157	0.0035	0.0097	0.0039	0.0015	0.0097	0.0060	0.0128	
CO_2i		0.0939	0.0133			0.1081	0.0292	0.0617	0.0951
(H_2S SO_2 COS)i	0.0163		0.0287	0.0034	0.002	0.0234	0.0026	0.0085	0.0033
PE							0.0165	0.0648	0.1222
PS							0.0001	0.0006	
PVC							0.2057	0.1922	0.012
PA							0.0356	0.0270	0.0891
PP							0.0041	0.0162	0.0305
H_2O_S	0.065	0.069	0.05[b]	0.01	0.01[b]	0.2[b]	0.13[b]	0.13[b]	0.275
ASH	0.003	0.002	0.6883	0.081	0.084	0.5957	0.0760	0.0666	0.166

[a]All values are in mass fraction on a wet basis. [b]Denotes assumed values.

because PE and PP have the same H/C ratio yet PE is more commonly found in waste mixtures,[56] e.g., bottles and bags, their ratio is preset here to 80:20, because a linear square fit would always result in a ratio of 50:50.

$$\mathrm{Bio}_1 = 0.6\mathrm{CELL} + 0.4\mathrm{HCE} \quad (26)$$

$$\mathrm{Bio}_2 = 0.2\mathrm{LIG}_C + 0.8\mathrm{LIG}_H \quad (27)$$

$$\mathrm{Bio}_3 = 0.2\mathrm{LIG}_C + 0.8\mathrm{LIG}_O \quad (28)$$

$$\mathrm{Bio}_N = 0.5\mathrm{PROT} + 0.5\mathrm{NH}_3\mathrm{i} \quad (29)$$

$$\mathrm{plastic}_1 = 0.8\mathrm{PE} + 0.2\mathrm{PP} \quad (30)$$

The remaining surrogate species are directly used as grid points (or matrix entries) for the interpolation: CO_2i, (H_2S SO_2 COS)i, PS, PVC, PA, and PP. The used grid points and represented areas are shown in Figure 6 for the mass ratio of hydrogen/carbon, oxygen/carbon, and nitrogen/carbon.

In addition to the fit of the elementary balance of the fuel, its ash and moisture contents known from proximate analyses are directly adopted. In case a biomass-derived fuel is considered (e.g., woody biomass or paper), all plastic species are excluded. The maximum content of plastic or biomass fraction is set here to 80 wt % to ensure a heterogeneous blend for waste mixtures. Examples of compiled surrogates are given in Table 6. The elementary composition of the surrogates represents well UCA of solid fuels for biomass (birch, spruce, and oil shale), paper-based mixtures (newspaper, cardboard, and paper sludge), and MSW. The LHV of surrogates is predicted within ±1.5 MJ/kg. The corresponding compositions of the surrogates are given in Table 7. If the references do not include the moisture content, typical values are assumed and denoted in the table. In case further information on the solid fuels are available, they are superimposed on the linear least squares fit, e.g., for MSW_1 and MSW_2, and the PVC amount of the waste mixture is known to be 24.6 and 23.3 wt % and set according to the surrogate composition (before the addition of ash and moisture contents).

Figure 7 shows the prediction of the stochastic reactor model against the TG curves using the surrogates from Tables 6 and 7 as well as their mixtures. The validation experiments cover biomass components (panels a and e of Figure 7), papers and their mixtures (panels b, c, and f of Figure 7), textile components (Figure 7d), and MSW and their blends (panels e and f of Figure 7). The weight loss of birch and spruce is well-predicted for low temperatures, while the final residue is slightly overpredicted (Figure 7a). However, the trend is kept well, which means that a delayed decomposition and higher residue with reference to birch is predicted for spruce. The decomposition of the newspaper is well-reproduced by the model. Its equal-weighted mixture with PVC shows a two-step decomposition as in the experiment but shifted slightly (Figure 7b). Milk and juice cartons are composite materials of cardboard, polyethylene, wax layers, and aluminum foil.[15] Milk cartons are modeled here by 90 wt % cardboard (Table 7) and 10 wt % PE, and juice cartons are modeled here by a mixture of 75 wt % cardboard, 20 wt % PE, and 5 wt % ash, instead of aluminum. Under low temperatures, the final residues of both carton types are well-predicted. However, the two-step decomposition seen in the experiments cannot be reproduced (Figure 7c). A possible explanation is that the only species in the surrogate set with a two-step decomposition is PVC, which is not included in the surrogate formulations for milk or juice cartons. The weight loss prediction of a textile component (modeled here as 90 wt % CELL and 10 wt % ash) replicates well the TG measurement of cotton fibers and the textile structure of a sweater.

In panels e and f of Figure 7, the weight loss prediction of MSW and their mixture with oil shale (OS) and paper sludge (PS) are provided. The MSW surrogates and their blends with paper sludge and oil shale are predicted in good agreement with the measurements. This validation shows that the weight loss rate and residue formation of various materials and complex waste mixtures can be well-predicted using the suggested surrogate species and decomposition scheme. These comparisons show that the formulated surrogates can reasonably well replicate the mass loss for single fractions of MSW (e.g., paper or textiles), biomass species and mixtures, and complex MSW mixtures.

2.3. Gas-Phase Reactions. Similar to the heterogeneous scheme, the secondary gas-phase reactions are also built from the biomass reaction scheme by Ranzi et al.[22] An extension is

https://dx.doi.org/10.1021/acs.energyfuels.0c03485
Energy Fuels 2021, 35, 7030−7049

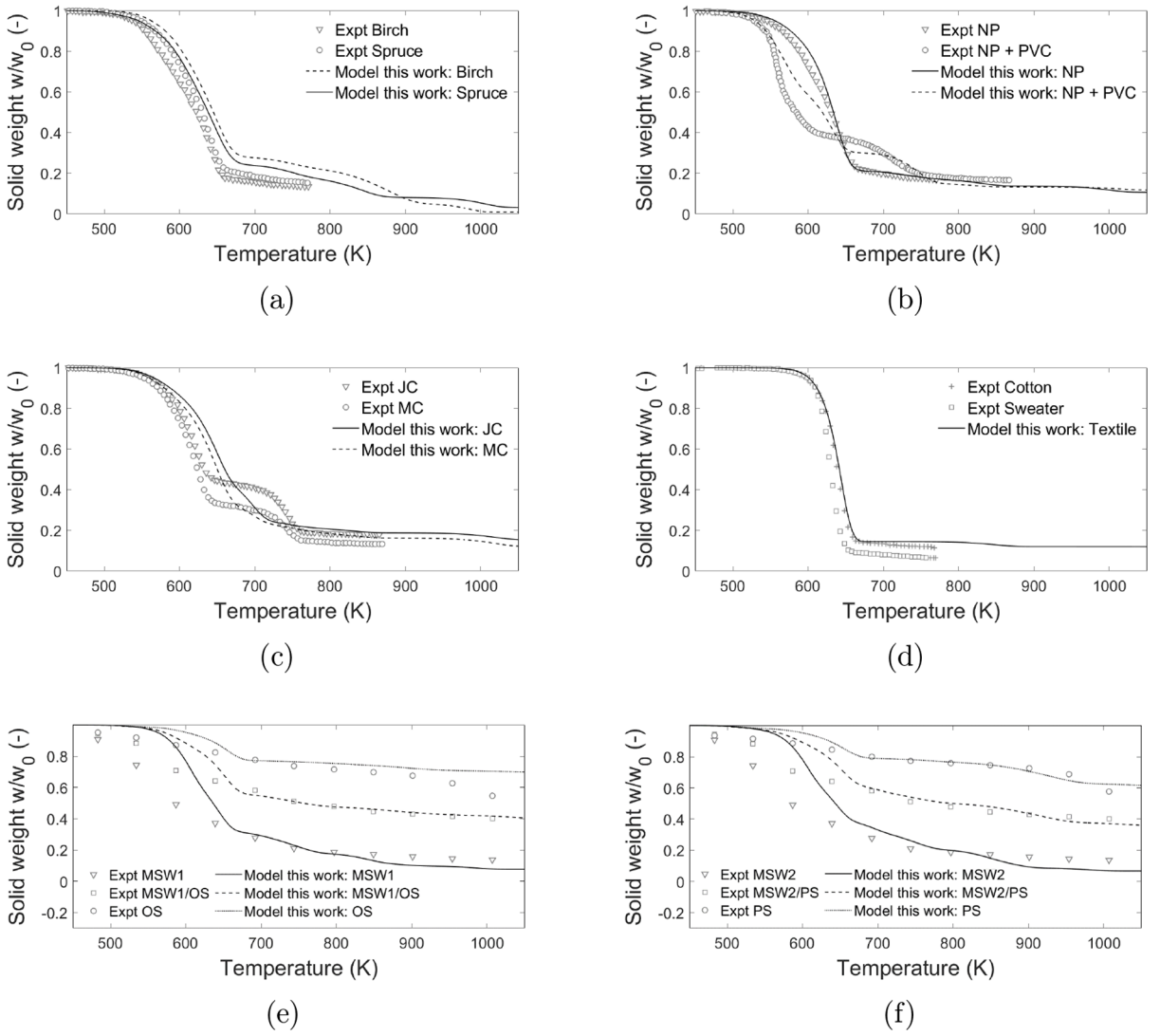

Figure 7. TG experimental curves for (a) birch and spruce at 10 K/min by SINTEF,[15] (b) newspaper (NP) and its blend with PVC (50 wt % each) at 10 K/min by SINTEF,[15] (c) juice carton (JC) and milk carton (MC) at 10 K/min by SINTEF,[15] (d) cotton fibers and cotton sweater at 10 K/min by SINTEF,[15] (e) oil shale (OS), MSW, and their mixture (50 wt % each) at 20 K/min by Fan et al.,[17] and (f) paper sludge (PS), MSW, and their blend (50 wt % each) at 20 K/min by Fang et al.[18] Model predictions show the solid mass loss of the corresponding initialized surrogate mixtures over the temperature range of 500−1000 K. The surrogate compositions are given in Table 7.

made by models that account for fuel NO_x, thermal NO_x, and prompt NO_x as well as sulfur and chlorine combustion. All included subsets are listed in Table 8. During the compilation and selection of reactions, thermodynamic, and transport data, a strict hierarchy is followed to keep the performance of the base mechanism. If a reaction and its reaction rates or species are present in the base mechanism, these data are adopted for the developed mechanism. If the reaction and species are new, the data from the highest ranked mechanism in Table 8 are used. Rank here means the appearance in descending order.

All selected subsets result in a detailed reaction scheme of 272 species and 3885 reactions. The model is reduced using the necessity analysis and reduction tools available in LOGEresearch[52] to save computational cost during the analysis of solid fuel conversion. Promising candidates for removal are identified by a low necessity N; here, $N > 0.001$. In the present model, the tar and gas species released by the solid surrogate and their further decomposition reactions are of special interest. Therefore, during the mechanism reduction, the speciation of each tar species and small hydrocarbons, directly released by the surrogate species, are compared against the detailed scheme and their corresponding reference scheme within each reduction step. If the removal of a certain species introduces a significant deviation from the detailed scheme, it is reintroduced. Additionally, the NO formation pathways are reviewed in every reduction step and validated against the literature measurements. The final scheme consists of 188 species and 3207 reactions and is described in the following. Pressure-dependent reactions (PLOG) are set to their reaction rates at atmospheric pressure as a result of the targeted application.

The biomass mechanism by Ranzi et al.[22] includes successive decomposition reactions of the released tar and gas species and their combustion reactions. It has pathways for typically formed species during solid fuel combustion, such as the previously discussed species released by the heterogeneous reaction model. Furthermore, known important intermediate species are included, e.g., furan (C_4H_4O). Details can be

https://dx.doi.org/10.1021/acs.energyfuels.0c03485
Energy Fuels 2021, 35, 7030−7049

Table 8. Included Mechanism and Selected Sub-models for the Gas-Phase Mechanism

reference	included species subset	description
Ranzi et al.[22]	full mechanism	oxidation of tar species and small hydrocarbons
Glarborg et al.[39]	NH_3 subset	NO and NO precursor chemistry
	amine subset	
	cyanide subset	
	CH_3CN subset	
	nitro and nitroso hydrocarbon subset	
	amino hydrocarbon subset	
Alzueta et al.[48]	pyridine subset	oxidation of pyridine and formation of NO precursors
Wu et al.[49]	pyrrole subset	oxidation of pyrrole and formation of NO precursors
Pelucchi et al.[69]	chlorine subset	chlorine gas-phase chemistry
Roesler et al.[34]	reactions for NO/HCl coupling	chlorine NO chemistry
Glarborg and Marshall[30]	COS/O_2 subset	sulfur gas-phase chemistry
	S subset, including H_2S	
Glarborg et al.[36]	reactions for SO_x−NO_x interactions	sulfur NO chemistry

found in the works by Ranzi and co-workers.[21,76] During the mechanism compilation, the performance of this mechanism is ensured in terms of the good prediction of ignition delay times (Figure 8) and speciation of small hydrocarbons for tar decomposition (Figure 9). In Figure 9b, a deviation of formed C_2H_2 between the reference mechanisms and the newly compiled scheme can be seen. This deviation results because of the introduction of the pyridine and pyrrole mechanisms (discussed in the following) and their interaction, e.g., in the acrylonitrile (CH_2CHCN) and acrylonitryl (CHCHCN) subsets.[48,49]

The mechanism is extended to account for NO_x precursors as well as the formation and transformation of NO_x. Several subsets from the mechanism by Glarborg et al.[39] are introduced. This mechanism is selected because it targets the modeling of nitrogen chemistry in combustion and can be considered state-of-the-art. All included subsets are listed in Table 8. The introduction of the subsets enables the fuel NO_x prediction from HCN and NH_3 and the interaction of nitrogen species with the hydrocarbon chemistry. Nitrogen-containing hydrocarbons with two C atoms or less, $C_{\leq 2}H_xN_x$, are covered by this scheme. The NO formation of the reference mechanism and the developed reaction schemes from N_2O and NNH (Figure 10a), from HCN (Figure 10b), and from NH_3 (Figure 10c) align well. The thermal NO_x and prompt NO_x predictions are shown in panels d and e of Figure 10. The thermal NO_x prediction reproduces well the reference mechanism and the experiment. However, prompt NO_x is underpredicted. The CH_4 chemistry and the radical pool differ between the mechanisms because the reactions by Ranzi et al.[22] are adopted for this work. Given the small absolute values of the experiment and the little contribution to

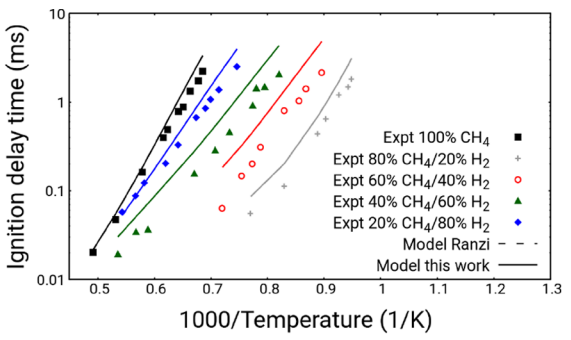

(a) IDT of different CH_4 / H_2 mixtures in O_2/AR at Φ=0.5, 20 atm by Zhang et al.[70]

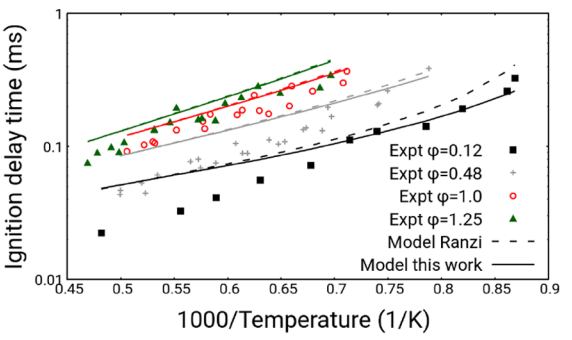

(b) IDT of C_2H_2 for varying Φ in O_2/AR at 1.18 to 1.21 bar by Eiteneer et al.[71]

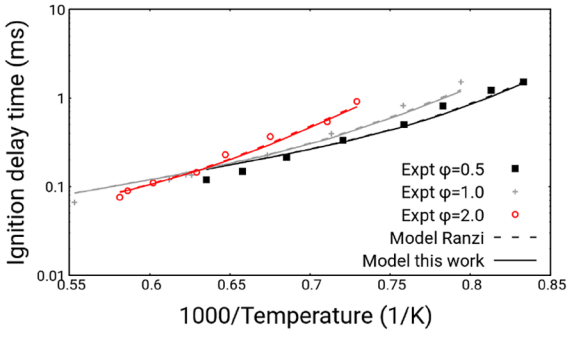

(c) IDT of C_2H_4 for varying Φ in O_2/AR at 1.17 bar by Mathieu et al.[72]

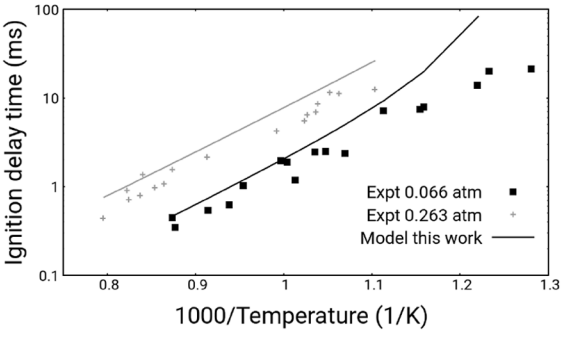

(d) IDT of a H_2/Cl_2 mixture in air at $\Phi = 0.3$ by Lifshitz and Schechner.[73]

Figure 8. Ignition delay time prediction of the developed reaction scheme versus experiments and reference reaction mechanisms.[70−73]

https://dx.doi.org/10.1021/acs.energyfuels.0c03485
Energy Fuels 2021, 35, 7030−7049

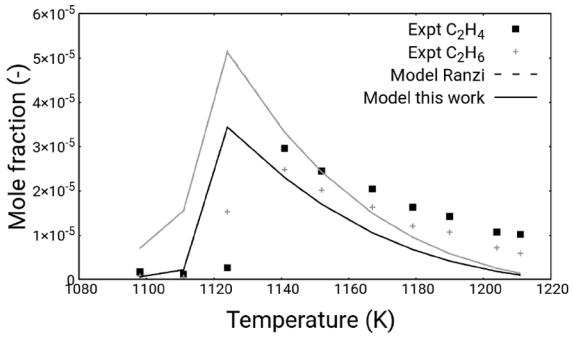

(a) C_2H_4 and C_2H_6 formation from CH_4 at Φ=0.1 and 1 atm in a N_2 atmosphere by Dagaut et al.[74]

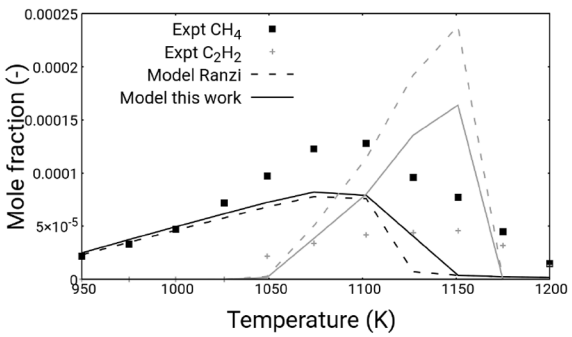

(b) CH_4 and C_2H_2 formation from 1700 ppm C_2H_4 at Φ=0.5 and 1 atm in a N_2 atmosphere by Cong et al.[75]

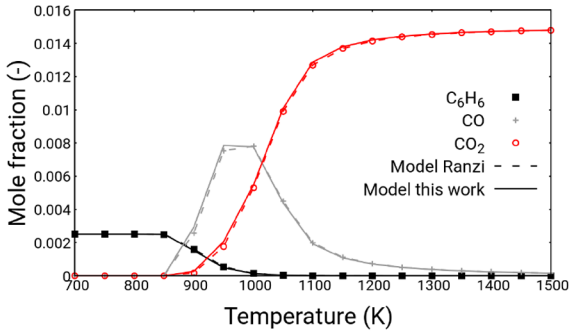

(c) Decomposition of C_6H_6 at Φ=0.1 and 1 atm in a N_2 atmosphere.

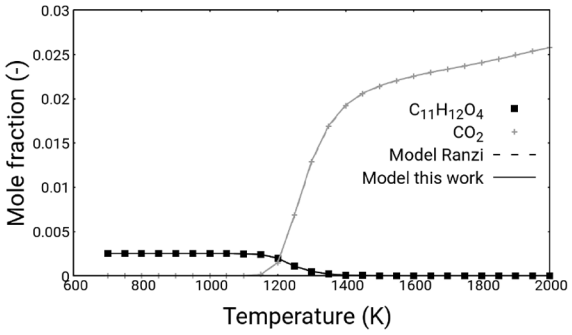

(d) Decomposition of $C_{11}H_{12}O_4$ at Φ=0.1 and 1 atm in a N_2 atmosphere.

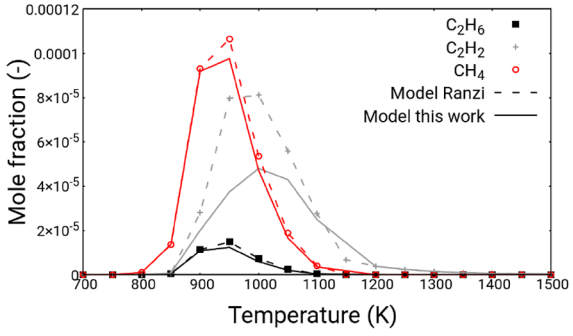

(e) Formation of CH_4, H_2 and CH_2HO by I-C_5H_{10} at Φ=0.1 and 1 atm in a N_2 atmosphere.

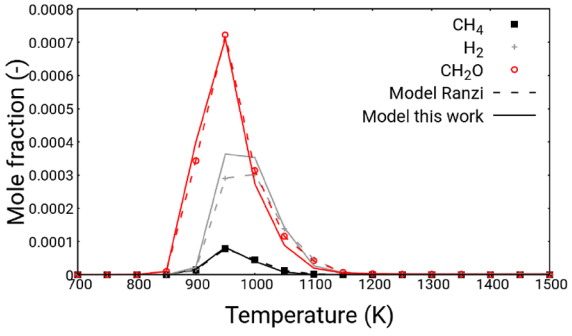

(f) Formation of CH_4, H_2 and CH_2O by $C_9H_{10}O_2$ at Φ=0.1 and 1 atm in a N_2 atmosphere.

Figure 9. Speciation of small hydrocarbons and selected >C_5 species compared to the reference mechanism by Ranzi et al.[22] Selected are two species released from the plastic surrogates (C_6H_6 and I-C_5H_{10}) and two from the biomass model ($C_{11}H_{12}O_4$ and $C_9H_{10}O_2$).[74,75]

NO formation from the prompt NO_x mechanism in waste combustion, the prediction is considered acceptable here. Further, the predicted NO reduction under selective non-catalytic reduction (SNCR) conditions for thermal deNO_x, rapereNO_x, and NO_xout is investigated. Small deviations between the mechanism by Glarborg et al.[39] and the presented scheme are visible, caused by a different radical pool. However, the general agreement and comparison to the experiments align well.

To model the thermal breakup of pyrrole and pyridine, reactions for their initiation and H abstraction reactions as well as reactions for $C_{3-5}H_xN_x$ species and their interaction with other gas-phase species are needed within the model. Therefore, the pyridine decomposition by Alzueta et al.[48] and additional pathways for pyridine decomposition and the pyrrole subset by Wu et al.[49] are added. The HCN formation under pyrolysis conditions by the two molecules is shown in Figure 11. The HCN formation prediction results from the pyrrole and pyridine subset in the combination of reactions

https://dx.doi.org/10.1021/acs.energyfuels.0c03485
Energy Fuels 2021, 35, 7030−7049

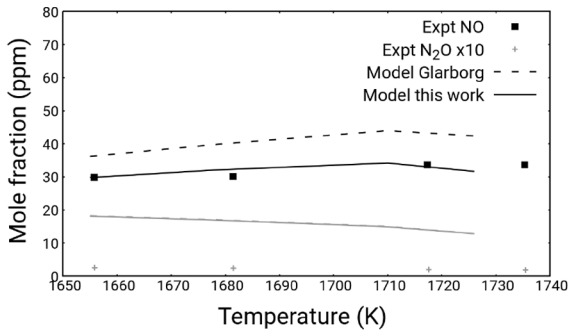

(a) NO and N_2O formation in a mixture of 17.4mol% CO, 82mol% air, 0.69–0.25mol% H_2 (decreasing with increasing temperature) at 1 atm by Stelee et al.[77]

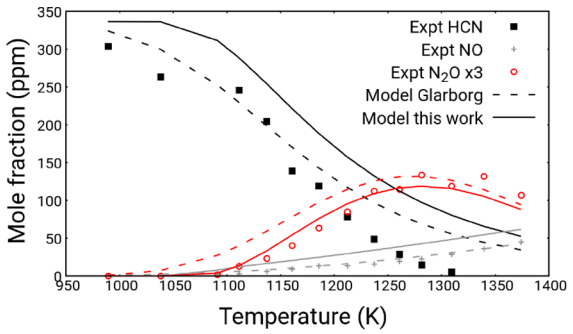

(b) NO formation from HCN in a mixture of 337 ppm HCN, 2.6mol% O_2, 3.1mol% H_20 in N_2 at 1 atm by Glarborg et al.[78]

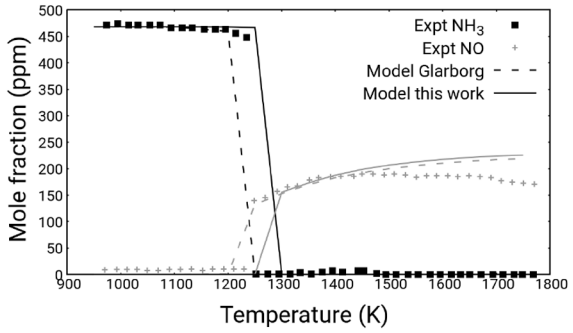

(c) NO formation from NH_3 in an stoichometric mixture of 2513 ppm CH_4, 468 ppm NH_3 and 5040 ppm O_2 in N_2 atmosphere by Mendiara et al.[79]

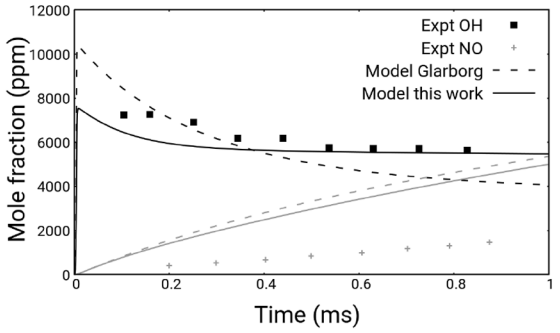

(d) Thermal NO formation in a mixture of 2mol% H_2, 6mol% O_2 and 92mol% N_2 at 2560 K and 2 bar by Bowman et al.[80]

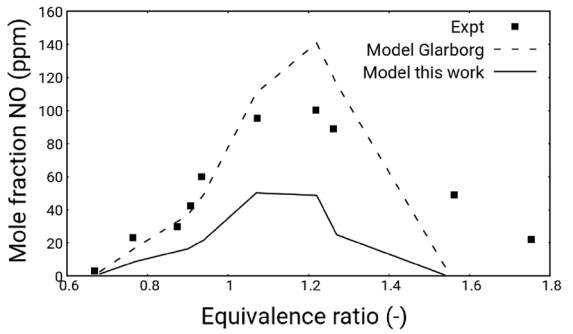

(e) Prompt NO formation in CH_4/air mixtures at 1 atm by Bartok et al.[81]

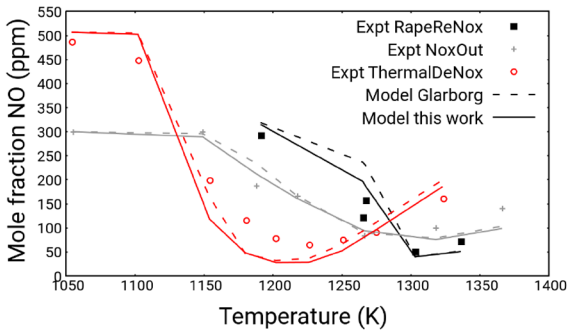

(f) SNCR conditions at 1 atm with NH_3 (Thermal DeNO$_X$) by Duo et al.,[82] with cyanuric acid (RapeReNO$_X$) by Caton et al.[83] and with urea (NO$_X$Out) by Alzueta et al. at[84]

Figure 10. Validation of the model prediction of the developed reaction mechanism against measurements and the reference scheme by Glarborg et al.[39,77−84]

from the model by Glarborg et al.,[39] which shows that the schemes link well together.

The model by Pelucchi et al.[69] that accounts for the high-temperature chemistry of HCl and Cl_2 is selected to predict further interaction with the gas phase of released HCl from PVC. This scheme accounts for the interaction of chlorine with OH, O, and H radicals, affecting the oxidation and reduction of the gas species and combustion products (CO and CO_2). Furthermore, the subset for NO/HCl coupling by

https://dx.doi.org/10.1021/acs.energyfuels.0c03485
Energy Fuels 2021, 35, 7030−7049

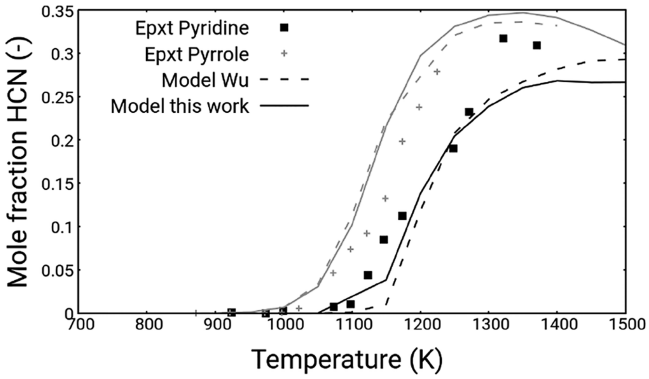

Figure 11. Predicted HCN formation by pyridine and pyrrole in argon at 1 atm against the model by Wu et al.[49] and experiments by Zhao et al.[85]

Roesler et al.[34] is added to link NO_x and chlorine chemistry directly.

$$NOCl + Cl = NO + Cl_2 \quad (31)$$

$$NOCl + H = NO + HCl \quad (32)$$

$$NOCl + O = ClO + NO \quad (33)$$

$$ClO + NO = NO_2 + Cl \quad (34)$$

$$HNO + Cl = HCl + NO \quad (35)$$

$$HONO + Cl = HCl + NO_2 \quad (36)$$

The model prediction of the CO reduction with the presence of HCl and the synergic impact of NO and HCl on its reduction are shown in Figure 12. For both experiments, the impact on CO chemistry by chlorine species is kept by the model.

Likewise, reactions for the sulfur-containing gas species released by inorganics are implemented. The main sulfur mechanism is taken from Glarborg and Marshall,[30] which is extended by SO_x and NO_x interaction reactions by Glarborg et al.[36]

$$SO + NO_2 = SO_2 + NO \quad (37)$$

$$SO_2 + NO_2 = SO_3 + NO \quad (38)$$

$$HSO + NO_2 = HOSO + NO \quad (39)$$

Figure 13 shows the well-captured speciation of COS and the reduction of CO in the presence of NO and SO_2 under SNCR conditions.

In summary, the developed reaction scheme offers good predictions for the presented experiments and the performance aligns with the reference mechanisms. The scheme describes the decomposition of tar species, including nitrogen- and oxygen-containing species and aromatics. Further, it includes the necessary NO_x formation and oxidation pathways and accounts for the interaction of emissions in the free board and under SNCR conditions.

3. APPLICATION

The developed reaction mechanism is applied to waste fuel bed simulations using the stochastic reactor network approach introduced by Netzer et al.[54] Several of the above-described stochastic gasification reactors are in this approach connected by *a priori* defined mass transfer. The approach is illustrated in Figure 14. For this analysis, the dimensions of a pilot plant for woody biomass waste by Razmjoo et al.[8] are applied. The surrogate fuel is fed to reactor 1 and mixed with fresh air; the conversion products are then transferred to reactor 2 and the released gas extracted; etc. A stochastic reactor represents the fuel bed above each grate bar with a length of 0.14 m. The bed width is 0.9 m, and the height is assumed to be 0.8 m. The mixing events are limited to one per time step to keep the heterogeneous character of the fuel bed. The results are compared to measurements and the outcome of an empirical model to understand the capabilities of the model. For this comparison, the NO_x precursor measurements by Jepsen et al.[6] at two operating conditions, corrosive species and NO measurement by Bøjer et al.,[7] and the empirical model by Jell et al.[9] serve as a reference. Because no UCA analysis is available for the studies by Bøjer et al.[7] and Jell et al.,[9] MSW1 and MSW3 (UCA analysis from Jepsen et al.[6]) are tested. The compositions are given in Table 7. For this comparison, the fuel bed length is normalized.

Figure 15 shows the prediction of the NO_x precursors HCN and NH_3 as well as NO releases along the fuel bed using MSW1. The predicted HCN aligns well with the empirical

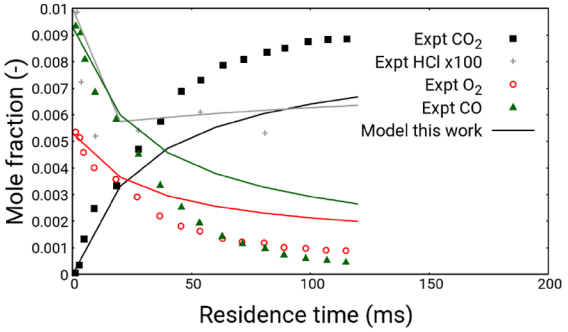

(a) Mixture of 0.93mol% CO, 0.53mol% O_2, 0.57mol% H_20 and 100ppm HCl in a N_2 atmosphere at 1010 K and 1 atm by Rösler et al.[86]

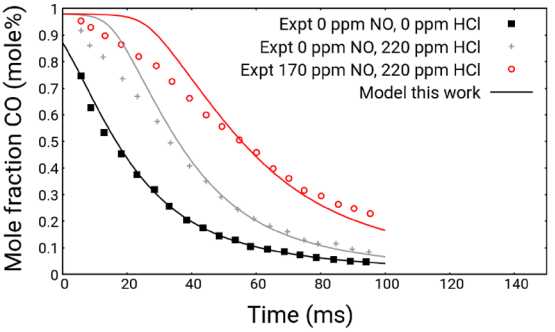

(b) Mixture of 0.97mol% CO, 0.5mol% O_2, 0.6mol% H_20 with traces of NO and HCl in a N_2 atmosphere at under stoichiometric conditions at 1005 K and 1 atm by Rösler et al.[34]

Figure 12. Validation of the developed reaction scheme for CO oxidation in a moist mixture under the presence of HCl and NO.[34,86]

https://dx.doi.org/10.1021/acs.energyfuels.0c03485
Energy Fuels 2021, 35, 7030−7049

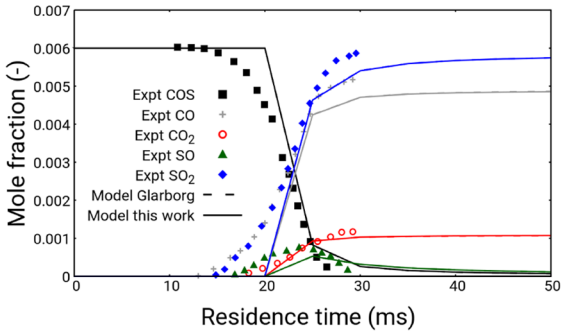

(a) SO_2 formation in a mixture of 0.6mol% COS and 6.6mol% O_2 at 1273 K and 0.0566 atm in an argon atmosphere by Glarborg et al.[87]

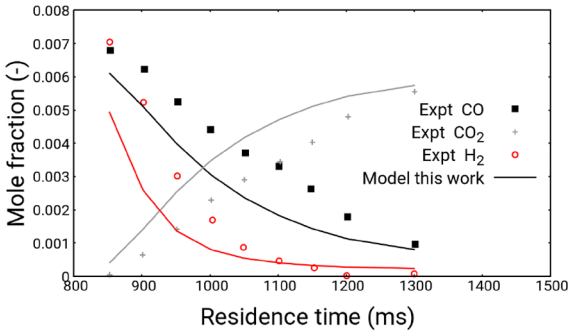

(b) Oxidation of CO under stoichiometric conditions in a mixture of 6500 ppm CO, 6500 ppm H_2, 950 ppm NO and 950 ppm SO_2 at 1 atm[29]

Figure 13. Model validation for the oxidation of COS and CO in the presence of SO_2 and NO.[29,87]

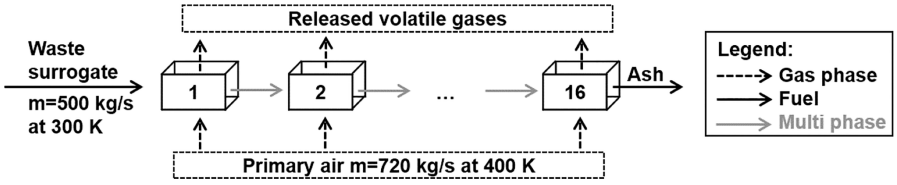

Figure 14. Illustration of the model approach for the fuel bed simulations.

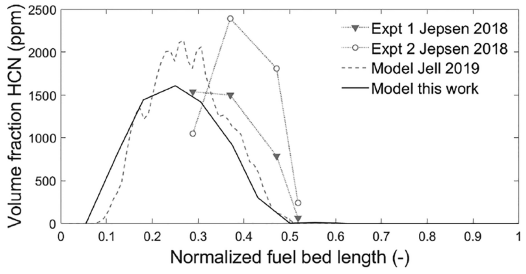

(a) Measurement of HCN by Jepsen et al.,[6] model by Jell et al.[9]

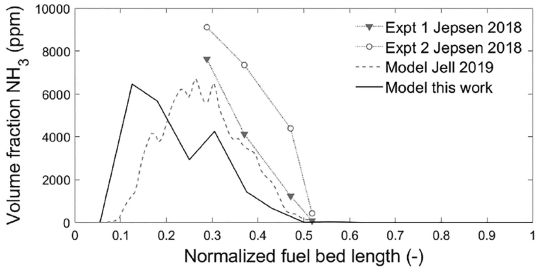

(b) Measurement of NH_3 by Jepsen et al.,[6] model by Jell et al.[9]

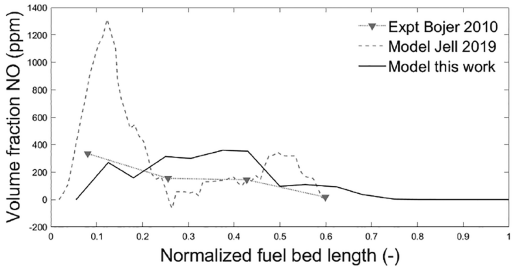

(c) Measurement of NO by Bøjer et al.,[7] model by Jell et al.[9]

Figure 15. Validation of the model prediction of released NO and NO_x precursors against measurements and an empirical model from the literature.

model and the measurements in terms of absolute numbers and range along the fuel bed.

The release of sulfur species is shown in Figure 16. From the experiment, the concentrations of sulfur and SO_2 are available. In the simulation, SO_2 is overpredicted because released H_2S and COS undergo further decomposition and oxidation, which result in SO_2 formation. However, in comparison to total released sulfur, the model prediction agrees in both magnitude and range of sulfur species.

The HCl release predicted using MSW1 and MSW3 are shown in Figure 17. The fuel bed range over which HCl is released is reproduced for both surrogates; however, the

https://dx.doi.org/10.1021/acs.energyfuels.0c03485
Energy Fuels 2021, 35, 7030−7049

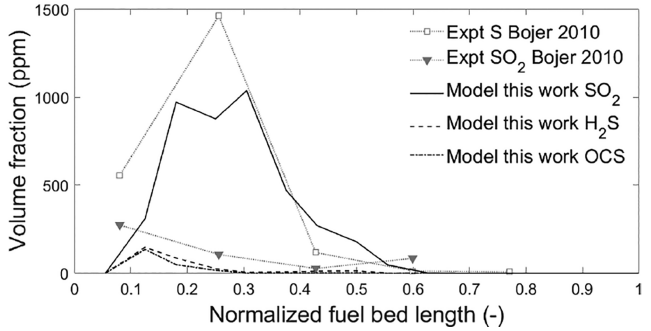

Figure 16. Validation of the predicted release of sulfur-containing species against measurements of SO_2 and sulfur by Bøjer et al.[7]

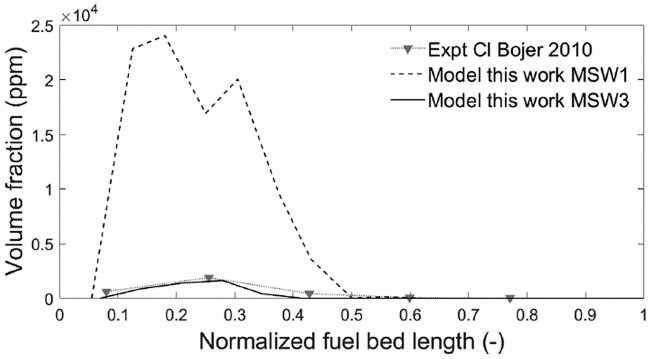

Figure 17. Validation of the predicted release of HCl against measurements by Bøjer et al.[7] for two different surrogates listed in Table 7.

absolute amount differs significantly. MSW1 has a high amount of PVC (20.6 wt %), whereas the amount of PVC in MSW3 is 1.2 wt %. This difference in the surrogate composition correlates directly to the released amount of HCl. Hence, for MSW1, HCl released is overpredicted but well-predicted for MSW3.

In summary, the developed reaction model and the fuel bed model can plausibly predict the release of emissions and their precursors. This prediction is sensitive to the used surrogate and, thus, the elementary composition of the waste mixture.

4. COMMENT ON LIMITATIONS AND POTENTIAL OF THE SURROGATE MODEL

As previously mentioned, the solid-phase description is based on single- and multi-step reactions that are of a global character. Particularly, the complex decomposition behavior of PE, PP, PS, and PA is simplified using a one-step reaction using experimentally obtained apparent reaction rates. Those experimentally obtained global reaction rates do not include the devolatilization only. They include all fundamental steps from the change within the melt, e.g., radical formation and changes in the molecular structure and morphology, and the release of large species (with carbon chains of >10 molecules). Further, the composition of the plastic species (eqs 9−12 and 22−25) are formulated to represent the typical range of released tar and gas as well as the solid residue. In devolatilization equations, the ratio is fixed, while in experiments, the ratio of these fractions and the included species vary. The variations are small compared to the biomass surrogate species and PVC that decompose over a significantly larger temperature range. It is assumed here to be negligible in the context of a surrogate model. In experiments, hundreds of different gas species can be measured during the thermal conversion of biomass, plastics, and waste mixtures. This variety cannot be reflected in a mathematical description for the simulations of engineering applications. Therefore, the released gas species have to be considered representative, and it has to be noted that this is not a fundamental description of a waste mixture. For example, chlorine is released from PVC in the model, while in WtE plants, e.g., food waste includes table salt (NaCl) that contributes to chlorine release. The origin of chlorine is not reflected in the model, while the overall released amount into the free board of a WtE can still be correctly represented by the model. The released gases of solid fuel combustion include tar species with large carbon chains of C_{10} and larger. Their general combustion behavior is modeled using smaller tar species with well-established reaction kinetics. This approach is indeed one of the fundamental assumptions of the concept of reference fuels, again, referring to liquid fuels, e.g., as complex diesel fuels represented by *n*-heptane, and the reference fuel for the octane number estimation is a blend of *n*-heptane and iso-octane, even though those fuels include species with $>C_{20}$ and aromatic species. In summary, a surrogate model aims to represent the key characteristic of a combustion process, while some (also fundamental phenomena) are not included in the model.

On the other side, using a surrogate model enables the formulation of a representative waste mixture for numerical investigations of a fuel that varies day by day and even hour by hour. Consequently, waste fuels are not as clearly specified as certain wood types, coal from a particular mine, or even transportation fuels. In comparison to the state-of-the-art practice to determine apparent kinetics for whole MSW mixtures or their fractions, a surrogate model overcomes the limitation of descriptive characteristics and moves toward a predictive description. Such models improve both the solid-phase description and the representation of tar species and emission precursors in the gas phase. As demonstrated in the Application section, the model can predict the release of key species compared to experiments and empirical models. In future work, the introduced model assumptions should be further validated using additional data from different waste incineration plants. The model should also be improved regarding the representative tar species, e.g., using caprolactam for the devolatilization of PA and the development of corresponding gas-phase chemistry.

In liquid fuel combustion, surrogates have been successfully used to represent liquid fuels for investigations such as the complex soot formation but also to generate reference fuels for experiments and engineering applications. With regard to waste management, different wastes may be mixed before burned in a WtE plant. In future work, the presented model should be used to study the effect of such mixing, aiming to optimize pollutant formation and thermal efficiency. In this way, the plant operation at predefined and optimum conditions could be maintained. Furthermore, the knowledge of changing waste fractions and their tendency to form emissions could be used for the control system to react faster to chaining emission formation.

5. CONCLUSION

A comprehensive kinetic model for the devolatilization of MSW is developed. The proposed model describes the MSW

https://dx.doi.org/10.1021/acs.energyfuels.0c03485
Energy Fuels 2021, 35, 7030−7049

solid fuel by the use of surrogate species, which include biomass species (cellulose, hemicellulose, and lignin species), protein, inorganic components that release CO_2, nitrogen species (NH_3 and NO), sulfur species (SO_2, H_2S, and COS), plastic species (PE, PS, PP, PA, and PVC), metaplastics, and char. A method for the surrogate formulation is presented and validated against TG measurements. A gas-phase mechanism for biomass is extended to account for fuel NO_x pathways, the combustion of pyrrole and pyridine as pyrolysis products of PA, and sulfur and chlorine combustion, which are pyrolysis products of PVC and inorganic species.

The formulation of the surrogate blend is based on the combination of a single surrogate species using a linear least squares fit. The mixture is fit to the elementary composition of UCA measurements of the analyzed solid fuel and its lower heating value. A good representation of the UCA guarantees a similar heat release in the model compared to the modeled application and a comparable amount of elements and their containing species that form gaseous emissions (N, S, and Cl).

The proposed heterogeneous reaction model can predict the weight loss of TG measurements for waste fractions, such as wood, textile, paper, and plastics, as well as different MSW mixtures. The developed gas-phase mechanism includes the description of tar and gas combustion, fuel NO_x precursors (HCN and NH_3), cyclic nitrogen hydrocarbons, and sulfur and chlorine interactions. All targeted NO_x formation and reduction pathways as well as operating conditions can be reproduced by the model. The developed reaction mechanism is applied in a reactor network model to simulate waste combustion in a grate-fired furnace. It shows good agreement with experiments and empirical devolatilization models.

Future work will address the validation toward varying operating conditions, such as primary air supply, flue gas recirculating, and temperatures. Furthermore, the model will be used to predict emissions in the free board of WtE plants, and critical kinetic pathways for the emission formation and reduction will be identified. On the basis of this analysis, the model will be used to develop measures for minimal fuel NO_x formation in grate-fired plants.

■ ASSOCIATED CONTENT

Supporting Information

The Supporting Information is available free of charge at https://pubs.acs.org/doi/10.1021/acs.energyfuels.0c03485.

Waste surrogate hetreogenous reactions (TXT)

Waste surrogate gas-phase mechanism (TXT)

Waste surrogate gas-phase thermodynamics (TXT)

Waste surrogate gas-phase transportation (TXT)

■ AUTHOR INFORMATION

Corresponding Author

Corinna Netzer − *Department of Energy and Process Engineering, Norwegian University of Science and Technology, 7491 Trondheim, Norway;* orcid.org/0000-0002-4445-7243; Email: corinna.netzer@ntnu.no

Authors

Tian Li − *Department of Energy and Process Engineering, Norwegian University of Science and Technology, 7491 Trondheim, Norway; RISE Fire Research, 7092 Tiller, Norway;* orcid.org/0000-0002-4248-8396

Terese Løvås − *Department of Energy and Process Engineering, Norwegian University of Science and Technology, 7491 Trondheim, Norway*

Complete contact information is available at: https://pubs.acs.org/10.1021/acs.energyfuels.0c03485

Notes

The authors declare no competing financial interest.

■ ACKNOWLEDGMENTS

The authors acknowledge the financial support by the Knowledge-Building Project GrateCFD (267957), funded by Statkraft Varme AS, EGE Oslo, Vattenfall AB, Hitachi Zosen Inova AG, Returkraft AS, and LOGE AB, together with the Research Council of Norway through the ENERGIX Program. UNINET Sigma2 and NTNU HPC Group provided high-performance computational resources.

■ REFERENCES

(1) Kaza, S.; Yao, L.; Bhada-Tata, P.; Woerden, F. V. *What a Waste 2.0—A Global Snapshot of Solid Waste Management to 2050*; World Bank Publications: Washington, D.C., 2018.

(2) Lu, J.-W.; Zhang, S.; Hai, J.; Lei, M. Status and perspectives of municipal solid waste incineration in China: A comparison with developed regions. *Waste Manage.* **2017**, *69*, 170−186.

(3) European Environmental Agency. *Annual Report 2009 and Environmental Statement 2010*; European Environmental Agency: Copenhagen, Denmark, 2010.

(4) Bogner, J.; Pipatti, R.; Hashimoto, S.; Diaz, C.; Mareckova, K.; Diaz, L.; Kjeldsen, P.; Monni, S.; Faaij, A.; Gao, Q.; Zhang, T.; Abdelrafie Ahmed, M.; Sutamihardja, R. T. M.; Gregory, R. Mitigation of global greenhouse gas emissions from waste: Conclusions and strategies from the Intergovernmental Panel on Climate Change (IPCC) Fourth Assessment Report. Working Group III (Mitigation). *Waste Manage. Res.* **2008**, *26* (1), 11−32.

(5) Glarborg, P.; Jensen, A.; Johnsson, J. Fuel nitrogen conversion in solid fuel fired systems. *Prog. Energy Combust. Sci.* **2003**, *29*, 89−113.

(6) Jepsen, M. S.; Jensen, P. A.; Clausen, S.; Fateev, A.; Glarborg, P.; Norman, T. Measurements of the NO_x precursors and major species concentrations above the grate at a waste-to-energy plant. *Fuel* **2018**, *222*, 475−484.

(7) Bøjer, M.; Jensen, P.; Dam-Johansen, K.; Madsen, O.; Lundtorp, K. Release of Corrosive Species above the Grate in a Waste Boiler and the Implication for Improved Electrical Efficiency. *Energy Fuels* **2010**, *24*, 5696−5707.

(8) Razmjoo, N.; Sefidari, H.; Strand, M. Measurements of temperature and gas composition within the burning bed of wet woody residues in a 4 MW moving grate boiler. *Fuel Process. Technol.* **2016**, *152*, 438−445.

(9) Jell, S.; von Raven, R.; Spliethoff, H. Untersuchung der Stickoxidminderung in der thermischen Müllverwertung. *Proceedings of 29th Deutscher Flammentag, German Section of the Combustion Institute*; Ruhr-Universität Bochum, Bochum, Germany, Sept 17−18, 2019; Paper IKV06.

(10) Frank, A.; Castaldi, M. CFD analysis of municipal solid waste combustion using detailed chemical kinetic modelling. *Waste Manage. Res.* **2014**, *32*, 745−754.

(11) Chhabra, V.; Shastri, Y.; Bhattacharya, S. Kinetics of Pyrolysis of Mixed Municipal Solid Waste-A Review. *Procedia Environ. Sci.* **2016**, *35*, 513−527.

(12) Sørum, L.; Grønli, M.; Hustad, J. Pyrolysis characteristics and kinetics of municipal solid wastes. *Fuel* **2001**, *80*, 1217−1227.

(13) Zheng, J.; Jin, Y. Q.; Chi, Y.; Wen, J. M. g; Jiang, X. G.; Ni, M. J. Pyrolysis characteristics of organic components of municipal solid waste at high heating rates. *Waste Manage.* **2009**, *29*, 1089−1094.

(14) Singh, S.; Wu, C.; Williams, P. T. Pyrolysis of waste materials using TGA-MS and TGA-FTIR as complementary characterisation techniques. *J. Anal. Appl. Pyrolysis* **2012**, *94*, 99−107.
(15) SINTEF Energy Research. *Characterisation of MSW for Combustion Systems*; SINTEF Energy Research: Trondheim, Norway, 2001; Technical Report STF-TR-A-5395.
(16) Grammelis, P.; Basinas, P.; Malliopoulou, A.; Sakellaropoulos, G. Pyrolysis kinetics and combustion characteristics of waste recovered fuels. *Fuel* **2009**, *88*, 195−205.
(17) Fan, Y.; Yu, Z.; Fang, S.; Lin, Y.; Lin, Y.; Liao, Y.; Ma, X. Investigation on the co-combustion of oil shale and municipal solid waste by using thermogravimetric analysis. *Energy Convers. Manage.* **2016**, *117*, 367−374.
(18) Fang, S.; Yu, Z.; Lin, Y.; Hu, S.; Liao, Y.; Ma, X. Thermogravimetric analysis of the co-pyrolysis of paper sludge and municipal solid waste. *Energy Convers. Manage.* **2015**, *101*, 626−631.
(19) Font, R.; Marcilla, A.; García, A.; Caballero, J.; Conesa, J. Kinetic models for the thermal degradation of heterogeneous materials. *J. Anal. Appl. Pyrolysis* **1995**, *32*, 29−39.
(20) Seo, M. W.; Kim, S. D.; Lee, S. H.; Lee, J. G. Pyrolysis characteristics of coal and RDF blends in non-isothermal and isothermal conditions. *J. Anal. Appl. Pyrolysis* **2010**, *88*, 160−167.
(21) Ranzi, E.; Cuoci, A.; Faravelli, T.; Frassoldati, A.; Migliavacca, G.; Pierucci, S.; Sommariva, S. Chemical Kinetics of Biomass Pyrolysis. *Energy Fuels* **2008**, *22*, 4292−4300.
(22) Ranzi, E.; Pierucci, S.; Aliprandi, P.; Stringa, S. Comprehensive and Detailed Kinetic Model of a Traveling Grate Combustor of Biomass. *Energy Fuels* **2011**, *25*, 4195−4205.
(23) Debiagi, P.; Pecchi, C.; Gentile, G.; Frassoldati, A.; Cuoci, A.; Faravelli, T.; Ranzi, E. Extractives Extend the Applicability of Multistep Kinetic Scheme of Biomass Pyrolysis. *Energy Fuels* **2015**, *29*, 6544−6555.
(24) Anca-Couce, A.; Mehrabian, R.; Scharler, R.; Obernberger, I. Kinetic scheme of biomass pyrolysis considering secondary charring reactions. *Energy Convers. Manage.* **2014**, *87*, 687−696.
(25) Anca-Couce, A. Reaction mechanisms and multi-scale modelling of lignocellulosic biomass pyrolysis. *Prog. Energy Combust. Sci.* **2016**, *53*, 41−79.
(26) Debiagi, P. E. A.; Trinchera, M.; Frassoldati, A.; Faravelli, T.; Vinu, R.; Ranzi, E. Algae characterization and multistep pyrolysis mechanism. *J. Anal. Appl. Pyrolysis* **2017**, *128*, 423−436.
(27) Žnidarčič, A.; Seljak, T.; Katrašnik, T. Surrogate model for improved simulations of small-scale sludge incineration plants. *Fuel* **2020**, *280*, 118422.
(28) Mehrabian, R.; Shiehnejadhesar, A.; Scharler, R.; Obernberger, I. Multi-physics modelling of packed bed biomass combustion. *Fuel* **2014**, *122*, 164−178.
(29) Dagaut, P.; Lecomte, F.; Mieritz, J.; Glarborg, P. Experimental and kinetic modeling study of the effect of NO and SO_2 on the oxidation of CO-H_2 mixtures. *Int. J. Chem. Kinet.* **2003**, *35*, 564−575.
(30) Glarborg, P.; Marshall, P. Oxidation of Reduced Sulfur Species: Carbonyl Sulfide. *Int. J. Chem. Kinet.* **2013**, *45*, 429−439.
(31) Chang, W.; Karra, S.; Senkan, S. A computational study of chlorine inhibition of CO flames. *Combust. Flame* **1987**, *69*, 113−122.
(32) Björkman, E.; Strömberg, B. Release of Chlorine from Biomass at Pyrolysis and Gasification Conditions1. *Energy Fuels* **1997**, *11*, 1026−1032.
(33) Wei, X.; Han, X.; Schnell, U.; Maier, J.; Wörner, H.; Hein, K. R. G. The Effect of HCl and SO_2 on NO_x Formation in Coal Flames. *Energy Fuels* **2003**, *17*, 1392−1398.
(34) Roesler, J. F.; Yetter, R. A.; Dryer, F. L. Kinetic interactions of CO, NO_x, and HCI emissions in postcombustion gases. *Combust. Flame* **1995**, *100*, 495−504.
(35) Zhao, J.; Wei, X.; Li, T.; Li, S. Effect of HCl and CO on nitrogen oxide formation mechanisms within the temperature window of SNCR. *Fuel* **2020**, *267*, 117231.
(36) Glarborg, P.; Kubel, D.; Dam-Johansen, K.; Chiang, H.-M.; Bozzelli, J. W. Impact of SO_2 and NO on CO oxidation under post-flame conditions. *Int. J. Chem. Kinet.* **1996**, *28*, 773−790.
(37) Malte, P.; Pratt, D. Measurement of atomic oxygen and nitrogen oxides in jet-stirred combustion. *Symp. (Int.) Combust., [Proc.]* **1975**, *15*, 1061−1070.
(38) Miller, J. A.; Bowman, C. T. Mechanism and modeling of nitrogen chemistry in combustion. *Prog. Energy Combust. Sci.* **1989**, *15*, 287−338.
(39) Glarborg, P.; Miller, J. A.; Ruscic, B.; Klippenstein, S. J. Modeling nitrogen chemistry in combustion. *Prog. Energy Combust. Sci.* **2018**, *67*, 31−68.
(40) Li, T.; Skreiberg; Løvås, T.; Glarborg, P. Skeletal mechanisms for prediction of NO_x emission in solid fuel combustion. *Fuel* **2019**, *254*, 115569.
(41) Shrestha, K. P.; Eckart, S.; Elbaz, A. M.; Giri, B. R.; Fritsche, C.; Seidel, L.; Roberts, W. L.; Krause, H.; Mauss, F. A comprehensive kinetic model for dimethyl ether and dimethoxymethane oxidation and NO_x interaction utilizing experimental laminar flame speed measurements at elevated pressure and temperature. *Combust. Flame* **2020**, *218*, 57−74.
(42) Faravelli, T.; Bozzano, G.; Colombo, M.; Ranzi, E.; Dente, M. Kinetic modeling of the thermal degradation of polyethylene and polystyrene mixtures. *J. Anal. Appl. Pyrolysis* **2003**, *70*, 761−777.
(43) Frassoldati, A.; Faravelli, T.; Ranzi, E. Kinetic modeling of the interactions between NO and hydrocarbons at high temperature. *Combust. Flame* **2003**, *135*, 97−112.
(44) Cuoci, A.; Frassoldati, A.; Faravelli, T.; Ranzi, E. Formation of soot and nitrogen oxides in unsteady counterflow diffusion flames. *Combust. Flame* **2009**, *156*, 2010−2022.
(45) Baawain, M.; Al-Mamun, A.; Omidvarborna, H.; Al-Amri, W. Ultimate composition analysis of municipal solid waste in Muscat. *J. Cleaner Prod.* **2017**, *148*, 355−362.
(46) Wu, C.-H.; Chang, C.-Y.; Hor, J.-L.; Shih, S.-M.; Chen, L.-W.; Chang, F.-W. On the thermal treatment of plastic mixtures of MSW: Pyrolysis kinetics. *Waste Manage.* **1993**, *13*, 221−235.
(47) Herrera, M.; Matuschek, G.; Kettrup, A. Main products and kinetics of the thermal degradation of polyamides. *Chemosphere* **2001**, *42*, 601−607.
(48) Alzueta, M. U.; Tena, A.; Bilbao, R. Pyridine conversion in a flow reactor and its interaction with nitric oxide. *Combust. Sci. Technol.* **2002**, *174*, 151−169.
(49) Wu, L.-N.; Tian, Z.-Y.; Weng, J.-J.; Yu, D.; Liu, Y.-X.; Tian, D.-X.; Cao, C.-C.; Zou, J.-B.; Zhang, Y.; Yang, J.-Z. Experimental and kinetic study on the low-temperature oxidation of pyridine as a representative of fuel-N compounds. *Combust. Flame* **2019**, *202*, 394−404.
(50) Zhao, C.; Jiang, E.; Chen, A. Volatile production from pyrolysis of cellulose, hemicellulose and lignin. *J. Energy Inst.* **2017**, *90*, 902−913.
(51) Francisca Gómez-Rico, M.; Font, R.; Fullana, A.; Martín-Gullón, I. Thermogravimetric study of different sewage sludges and their relationship with the nitrogen content. *J. Anal. Appl. Pyrolysis* **2005**, *74*, 421−428.
(52) LOGE AB. *LOGEsoft v1.10*; LOGE AB: Lund, Sweden, 2020; http://www.logesoft.com.
(53) Weber, K.; Li, T.; Løvås, T.; Perlman, C.; Seidel, L.; Mauss, F. Stochastic reactor modeling of biomass pyrolysis and gasification. *J. Anal. Appl. Pyrolysis* **2017**, *124*, 592−601.
(54) Netzer, C.; Li, T.; Seidel, L.; Mauß, F.; Løvås, T. Stochastic Reactor-Based Fuel Bed Model for Grate Furnaces. *Energy Fuels* **2020**, *34*, 16599−16612.
(55) Attar, A. Chemistry, thermodynamics and kinetics of reactions of sulphur in coal-gas reactions: A review. *Fuel* **1978**, *57*, 201−212.
(56) Zhou, H.; Meng, A.; Long, Y.; Li, Q.; Zhang, Y. Classification and comparison of municipal solid waste based on thermochemical characteristics. *J. Air Waste Manage. Assoc.* **2014**, *64*, 597−616.
(57) Duan, L.; Zhao, C.; Zhou, W.; Qu, C.; Chen, X. Investigation on Coal Pyrolysis in CO_2 atm. *Energy Fuels* **2009**, *23*, 3826−3830.

https://dx.doi.org/10.1021/acs.energyfuels.0c03485
Energy Fuels 2021, 35, 7030−7049

(58) Zhou, Q.; Hu, H.; Liu, Q.; Zhu, S.; Zhao, R. Effect of Atmosphere on Evolution of Sulfur-Containing Gases during Coal Pyrolysis. *Energy Fuels* **2005**, *19*, 892−897.
(59) Mehl, M.; Marongiu, A.; Faravelli, T.; Bozzano, G.; Dente, M.; Ranzi, E. A kinetic modeling study of the thermal degradation of halogenated polymers. *J. Anal. Appl. Pyrolysis* **2004**, *72*, 253−272.
(60) Faravelli, T.; Pinciroli, M.; Pisano, F.; Bozzano, G.; Dente, M.; Ranzi, E. Thermal degradation of polystyrene. *J. Anal. Appl. Pyrolysis* **2001**, *60*, 103−121.
(61) Marongiu, A.; Faravelli, T.; Bozzano, G.; Dente, M.; Ranzi, E. Thermal degradation of poly(vinyl chloride). *J. Anal. Appl. Pyrolysis* **2003**, *70*, 519−553.
(62) López, A.; de Marco, I.; Caballero, B.; Laresgoiti, M.; Adrados, A. Influence of time and temperature on pyrolysis of plastic wastes in a semi-batch reactor. *Chem. Eng. J.* **2011**, *173*, 62−71.
(63) Anuar Sharuddin, S. D.; Abnisa, F.; Wan Daud, W. M. A.; Aroua, M. K. A review on pyrolysis of plastic wastes. *Energy Convers. Manage.* **2016**, *115*, 308−326.
(64) Michal, J.; Mitera, J.; Kubat, J. Major Pyrolysis and Thermoxidative Products from Certain Polyamides. *Fire Mater.* **1981**, *5*, 1−5.
(65) Bockhorn, H.; Donner, S.; Gernsbeck, M.; Hornung, A.; Hornung, U. Pyrolysis of polyamide 6 under catalytic conditions and its application to reutilization of carpets. *J. Anal. Appl. Pyrolysis* **2001**, *58*−*59*, 79−94.
(66) Anthony, G. M. Kinetic and chemical studies of polymer cross-linking using thermal gravimetry and hyphenated methods. Degradation of polyvinylchloride. *Polym. Degrad. Stab.* **1999**, *64*, 353−357.
(67) Cuoci, A.; Faravelli, T.; Frassoldati, A.; Granata, S.; Migliavacca, G.; Pierucci, S.; Ranzi, E.; Sommariva, S. A General Mathematical Model of Biomass Devolatilization. Note 2. Detailed Kinetics of Volatile Species. *Proceedings of the 30th Meeting on Combustion, Italian Section of the Combustion Institute*; Ischia, Italy, June 20−22, 2007.
(68) FEC Consultants. *Forestry Waste Firing of Industrial Boilers*; FEC Consultants: Oldham, U.K., 1990; ETSU-B-1178.
(69) Pelucchi, M.; Frassoldati, A.; Faravelli, T.; Ruscic, B.; Glarborg, P. High-temperature chemistry of HCl and Cl2. *Combust. Flame* **2015**, *162*, 2693−2704.
(70) Zhang, Y.; Huang, Z.; Wei, L.; Zhang, J.; Law, C. Experimental and modeling study on ignition delays of lean mixtures of methane, hydrogen, oxygen, and argon at elevated pressures. *Combust. Flame* **2012**, *159*, 918−931.
(71) Eiteneer, B.; Frenklach, M. Experimental and modeling study of shock-tube oxidation of acetylene. *Int. J. Chem. Kinet.* **2003**, *35*, 391−414.
(72) Mathieu, O.; Goulier, J.; Gourmel, F.; Mannan, M.; Chaumeix, N.; Petersen, E. Experimental study of the effect of CF3I addition on the ignition delay time and laminar flame speed of methane, ethylene, and propane. *Proc. Combust. Inst.* **2015**, *35*, 2731−2739.
(73) Lifshitz, A.; Schechner, P. The mechanism of the H_2 + Cl_2 reaction: Ignition behind reflected shocks. *Int. J. Chem. Kinet.* **1975**, *7*, 125−142.
(74) Dagaut, P.; Boettner, J.; Cathonnet, M. Methane Oxidation: Experimental and Kinetic Modeling Study. *Combust. Sci. Technol.* **1991**, *77*, 127−148.
(75) Cong, T.; Bedjanian, E.; Dagaut, P. Oxidation of Ethylene and Propene in the Presence of CO_2 and H_2O: Experimental and Detailed Kinetic Modeling Study. *Combust. Sci. Technol.* **2010**, *182*, 333−349.
(76) Ranzi, E.; Dente, M.; Goldaniga, A.; Bozzano, G.; Faravelli, T. Lumping procedures in detailed kinetic modeling of gasification, pyrolysis, partial oxidation and combustion of hydrocarbon mixtures. *Prog. Energy Combust. Sci.* **2001**, *27*, 99−139.
(77) Steele, R. C.; Malte, P. C.; Nicol, D. G.; Kramlich, J. C. NO_x and N_2O in lean-premixed jet-stirred flames. *Combust. Flame* **1995**, *100*, 440−449.
(78) Glarborg, P.; Miller, J. A. Mechanism and modeling of hydrogen cyanide oxidation in a flow reactor. *Combust. Flame* **1994**, *99*, 475−483.
(79) Mendiara, T.; Glarborg, P. Ammonia chemistry in oxy-fuel combustion of methane. *Combust. Flame* **2009**, *156*, 1937−1949.
(80) Bowman, C. T. Investigation of Nitric Oxide Formation Kinetics in Combustion Processes: The Hydrogen-Oxygen-Nitrogen Reaction. *Combust. Sci. Technol.* **1971**, *3*, 37−45.
(81) Bartok, W.; Engleman, V.; Goldstein, R.; Valle, E. D. Basic kinetic studies and modeling of nitrogen oxide formation in combustion progresses. *AIChE Symp. Ser.* **1972**, *68* (126), 30−38.
(82) Duo, W. Kinetic studies of the reactions involved in selective non-catalytic reduction of nitric oxide. Ph.D. Thesis, Technical University of Denmark, Kongens Lyngby, Denmark, 1990.
(83) Caton, J. A.; Siebers, D. L. Comparison of Nitric Oxide Removal by Cyanuric Acid and by Ammonia. *Combust. Sci. Technol.* **1989**, *65*, 277−293.
(84) Alzueta, M. U.; Røjel, H.; Kristensen, P. G.; Glarborg, P.; Dam-Johansen, K. Laboratory Study of the $CO/NH_3/NO/O_2$ System: Implications for Hybrid Reburn/SNCR Strategies. *Energy Fuels* **1997**, *11*, 716−723.
(85) Zhao, Q.; Wang, X.; Tan, H.; Si, J.; Niu, Y.; Xu, T. Co-pyrolysis of Pyridine and Pyrrole as Nitrogenous Compounds Model of Coal. *Asian J. Chem.* **2010**, *22*, 6998−7004.
(86) Roesler, J. F.; Yetter, R. A.; Dryer, F. L. Detailed Kinetic Modeling of Moist CO Oxidation Inhibited by Trace Quantities of HCl. *Combust. Sci. Technol.* **1992**, *85*, 1−22.
(87) Glarborg, P.; Marshall, P. Oxidation of Reduced Sulfur Species: Carbonyl Sulfide. *Int. J. Chem. Kinet.* **2013**, *45*, 429−439.

https://dx.doi.org/10.1021/acs.energyfuels.0c03485
Energy Fuels 2021, 35, 7030−7049